INORGANIC CHEMISTRY FRONTIERS

RESEARCH ARTICLE

View Article Online
View Journal | View Issue

Cite this: *Inorg. Chem. Front.*, 2025, **12**, 7083

Heterometallic calcium–alkali metal aryloxides as catalysts for the solvothermal alcoholysis of nylon-6 waste†

Rafał Petrus, *[a] Karolina Matuszak,[a] Adrian Kowaliński [a] and Tadeusz Lis[b]

In this study, we report the synthesis of homometallic and heterometallic calcium aryloxides: $[Ca(sal\text{-}Me)_2(MeOH)]_n$ (**1**), $[Ca_3(sal\text{-}Me)_6(MeOH)_2]$ (**2**), $[Ca_2Li_2(sal\text{-}Me)_6(THF)_2]$ (**3**), $[Ca_2Na_2(sal\text{-}Me)_6(MeOH)_4]$ (**4**), and $[Ca_2K_2(sal\text{-}Me)_6(MeOH)_4]$ (**5**). Compounds **1** and **2** were obtained *via* direct reaction of metallic calcium with methyl salicylate (Hsal-Me) in methanol (MeOH). A similar synthetic route, incorporating one equivalent of an alkali metal (M′ = Li, Na, K) and tetrahydrofuran (THF), was used to obtain the heterometallic derivatives **3–5**. A central focus of this work is the synthesis of heterometallic Ca^{2+}–M'^{+} complexes, of which only 13 examples have been previously documented. A detailed investigation of the reaction pathways led to the identification of intermediate compounds: $[Ca_3(sal\text{-}Me)_6(THF)_4]$ (**2a**), $[CaLi_6(sal\text{-}Me)_8]$ (**6**), and $[Ca_3Na_4(sal\text{-}Et)_{10}(Hsal\text{-}Et)_2]$ (**7**) (Hsal-Et = ethyl salicylate). Additionally, reactions conducted under atmospheric moisture conditions yielded the uncommon pentanuclear complexes $[Ca_4Na(\mu_5\text{-}OH)(sal\text{-}Et)_8(MeOH)]$ (**8**) and $[Ca_4K(\mu_5\text{-}OH)(sal\text{-}Et)_8(EtOH)]$ (**9**). Compounds **1–9**, along with previously reported $[M'_6(sal\text{-}Me)_6]$ (M'^{+} = Li^+(**10**), Na^+(**11**), K^+(**12**)), $[Mg_2(sal\text{-}Et)_4(EtOH)_2]$ (**13**), $[Zn_4(sal\text{-}Me)_8]$ (**14**), $[M_2M'_2(sal\text{-}Me)_6(THF)_x]$ (M^{2+} = Mg^{2+}; M'^{+} = Li^+(**15**), Na^+(**16**), K^+(**17**); M^{2+} = Zn^{2+}; M'^{+} = Li^+(**18**), Na^+(**19**), K^+(**20**); x = 0, 2, 4), and $[Mg_4Na_2(sal\text{-}Me)_6(sal)_2(THF)_4]$ (**21**) were evaluated as catalysts for the chemical recycling of polyamide waste. Among them, the heterometallic catalysts **3**, **6**, and **18–20** exhibited the highest catalytic activity in the methanolysis of nylon-6 at 220 °C. Particular emphasis is placed on the reaction conditions and the high efficiency of the catalysts.

Received 22nd April 2025,
Accepted 28th June 2025

DOI: 10.1039/d5qi00994d

rsc.li/frontiers-inorganic

Introduction

Over the past few decades, research on the chemical and structural properties of calcium compounds has been largely overshadowed by that of its lighter congener, magnesium. Most studies have focused on calcium alkyl, hydrido, amido, and alkoxido complexes, primarily investigated as catalysts in organic synthesis,[1–4] or the polymerization of activated alkenes.[5] Due to their strong permeability, high reactivity, good film-forming capabilities, and consolidation properties, calcium alkoxides have found applications as Ca^{2+} precursors in the synthesis of $CaCO_3$ for cultural heritage conservation,[6–8] SiO_2–CaO bioactive glasses for medical technologies,[9] and synthetic rock waste (Synroc), such as zirconolite ($CaZrTi_2O_7$) and perovskite ($CaTiO_3$) for immobilizing high-level radioactive waste.[10]

In contrast, calcium aryloxides have received significantly less attention despite their practical relevance. These calcium derivatives have been used as additives in lubricating oils, acting as detergents to disperse sludge, reduce corrosion, and maintain engine cleanliness.[11–13] Sulfurized calcium alkyl phenolates are also employed in the production of environmentally friendly packaging materials.[14,15] Moreover, calcium phenoxides have been studied for wood preservation, as active adhesives in bitumen,[16] and even as insecticides.[17,18] The reaction between CaO and phenols has been employed to remove concentrated aromatic hydroxy compounds from wastewater, achieving removal rates as high as 85.5%.[19] Additionally, a calcium compound formed by the reaction of 1,3-butylene glycol disalicylate with $Ca(OH)_2$ has been identified as a component in the self-setting dental cement Dycal®.[20] Boyle and colleagues also explored the use of tetranuclear $[Ca_4(\mu_3\text{-}OH)_2(\mu\text{-}OAr)_4(OAr)_2(THF)_6]$ (ArO^- = 2,6-dimethylphenolato) and mononuclear $[Ca(OAr)_2(THF)_x]$ (ArO^- = 2,6-diisopropylphenolato; x = 3, 4) aryloxides as molecular precursors for the synthesis of portlandite ($Ca(OH)_2$) and vaterite ($CaCO_3$), respectively.[21]

[a]*Faculty of Chemistry, Wrocław University of Science and Technology, 23 Smoluchowskiego, 50-370 Wrocław, Poland. E-mail: rafal.petrus@pwr.edu.pl*
[b]*Faculty of Chemistry, University of Wrocław, 14 F. Joliot-Curie, 50-383 Wrocław, Poland*

† Electronic supplementary information (ESI) available. CCDC 2420420–2420427. For ESI and crystallographic data in CIF or other electronic format see DOI: https://doi.org/10.1039/d5qi00994d

The development of catalytic transformations based on earth-abundant, non-toxic, and inexpensive early main-group metals is essential for establishing sustainable alternatives to transition-metal-based catalysis.[22,23] Despite their economic and environmental advantages, the catalytic applications of calcium aryloxides remain underexplored. Their use has been largely confined to the ring-opening polymerization (ROP) of cyclic esters, such as L- or *rac*-lactide (L-LA or *rac*-LA).[24–30] For example, $[Ca(BHT)_2(THF)_3]$ and $[Ca(EDP)(THF)_2]_2$ initiate the polymerization of L-LA with 84–93% conversion in 1.5–4 minutes (L-LA/I/BnOH = 100/0.1/1 in toluene), yielding PLLA with number-average molecular weight (M_n) values of 12.1 and 13.4 kDa, and dispersity ($Đ$) of 1.08 and 1.25, respectively.[31] Another notable example is the ionic complex $[Ca(L)][H_2N\{B(C_6F_5)_3\}_2]$ (L^- = 2-[(1,4,7,10-tetraoxa-13-azacyclopentadecan-13-yl)methyl]-4,6-di-*tert*-butylphenolato), which reached 96% conversion of L-LA after 24 h (L-LA/I/BnOH = 300/0.1/1 in toluene at 60 °C), producing PLLA with M_n of 30.0 kDa and $Đ$ of 1.06.[32]

In organic synthesis, catalytically active calcium aryloxide species remain poorly defined and are typically generated *in situ* by combining $Ca(OR)_2$ with biphenolate ligands. These species have been applied in various reactions, including transesterifications,[33] amine–borane dehydrogenations,[34] enantioselective 1,4-addition of malonates to nitroalkenes,[35] asymmetric Baylis–Hillman reactions,[36] asymmetric epoxidation of α,β-unsaturated enones,[37] and asymmetric Michael additions.[38,39]

While the synthesis of simple calcium aryloxides is well established,[40–45] reports on well-characterized heterobimetallic calcium–alkali metal complexes remain scarce due to their tendency to form mixtures of homometallic species or structurally diverse mixed-metal aggregates.[46–48] Recently, heterometallic cooperativity involving s-block elements has attracted growing interest, as such systems often demonstrate enhanced catalytic activity and selectivity compared to their homometallic counterparts.[49] However, no studies to date have addressed the use of heterometallic calcium–alkali metal complexes as catalysts in organic synthesis, polymerization of heterocyclic monomers, or the chemical recycling of plastics.

In this context, our focus is primarily on the chemical recycling of polyamide 6 (PA6), one of the most widely used thermoplastic polymers, known for its high thermal and mechanical resistance, tensile strength, and excellent chemical resistance to acids and alkalis. These properties make it suitable for diverse applications, including construction, automotive, textiles, and separation processes.[50,51] However, due to its excellent chemical and thermal stability, recycling post-consumer PA6 presents a significant challenge. Mechanical recycling is a common method for PA6 recycling because of its lower cost, shorter processing time, reduced carbon footprint, and lower environmental impact. However, it often results in degradation and deterioration of the material's properties.[52] In contrast, chemical recycling breaks down the polymer chain into monomers, oligomers, or other low-molecular-weight derivatives, making it a viable option for plastics that are no longer suitable for mechanical recycling.[53] Various chemical depolymerization routes have been explored for PAs, including pyrolysis, hydrolysis, hydrogenolysis, ammonolysis, aminolysis, and alcoholysis. Generally, PA6 chemical recycling requires high temperatures (270–320 °C), high-pressure steam, long reaction times, sub- and supercritical water/ammonia/amines/alcohols, acid or base reagents, and efficient catalysts (*e.g.*, inorganic acids, organic acids/bases, metal salts, or hydroxides).[54–57] Most studies focus on PA6 depolymerization to recover ε-caprolactam (CL), the cyclic monomer, which is subsequently isolated *via* distillation (ESI, section: Chemical recycling of PA6†).[58] The development of new catalytic systems enabling the recovery of value-added chemicals from polymer waste has attracted increasing attention in the fields of environmental impact, plastic recycling technologies, catalysis, and fine chemical production.

In this study, we report the synthesis of a one-dimensional coordination polymer, $[Ca(sal\text{-}Me)_2(MeOH)]_n$ (**1**), and a trinuclear calcium compound, $[Ca_3(sal\text{-}Me)_6(MeOH)_2]$ (**2**), *via* direct reaction of metallic calcium with two equivalents of methyl salicylate (Hsal-Me) in MeOH, followed by crystallization from concentrated or diluted methanolic solutions. Particular focus was placed on synthesizing heterometallic Ca^{2+}–M'^{+} compounds, achieved by reacting metallic Ca with Hsal-Me (1 : 3), followed by the addition of one equivalent of an alkali metal (M′ = Li, Na, K). This approach yielded heterometallic aryloxides: $[Ca_2Li_2(sal\text{-}Me)_6(THF)_2]$ (**3**), $[Ca_2Na_2(sal\text{-}Me)_6(MeOH)_4]$ (**4**), and $[Ca_2K_2(sal\text{-}Me)_6(MeOH)_4]$ (**5**). Detailed reaction analysis revealed the formation of intermediates such as $[Ca_3(sal\text{-}Me)_6(THF)_4]$ (**2a**), $[CaLi_6(sal\text{-}Me)_8]$ (**6**), and $[Ca_3Na_4(sal\text{-}Et)_{10}(Hsal\text{-}Et)_2]$ (**7**) (Hsal-Et = ethyl salicylate) during the synthesis of **3–5**. When reactions were conducted with a fourfold molar excess of Ca relative to metallic Na or K, and using eight equivalents of Hsal-Me in a ROH/THF solution, exposure to atmospheric moisture or the deliberate addition of water led to the formation of pentanuclear $[Ca_4Na(\mu_5\text{-}OH)(sal\text{-}Et)_8(MeOH)]$ (**8**) and $[Ca_4K(\mu_5\text{-}OH)(sal\text{-}Et)_8(EtOH)]$ (**9**). The catalytic potential of compounds **1–9** was evaluated in the chemical recycling of polyamide waste.

Results and discussion

Synthesis and structural characterization of homometallic and heterometallic calcium aryloxides

The direct reaction of metallic calcium with two equivalents of methyl salicylate (Hsal-Me) in methanol resulted in the formation of a one-dimensional coordination polymer, $[Ca(sal\text{-}Me)_2(MeOH)]_n$ (**1**, 59%), in which aryloxide oxygen atoms of the ligands bridge Ca^{2+} ions. Bis(phenolato)calcium coordination polymers are uncommon, with only four examples reported to date: $[Ca(OAr)_2(H_2O)_x]_n$ (ArO^- = 2-nitrophenolate, 4-nitrophenolate; x = 1, 2), $\{[Ca(\mu\text{-}H_2O)_2(OAr)(H_2O)_2]OAr\}_n$, and $[Ca_3(OAr)_6(H_2O)_2]_n$ (ArO^- = 2,5-dihydroxy-3,6-diisopropyl-*p*-benzoquinone).[59] Calcium coordination polymers are more commonly formed using phenolic carboxylate ligands, such as $[Ca(bdda)(H_2O)_2]_n$ ($bdda^{2-}$ = benzene-1,3-dioxydiacetate;

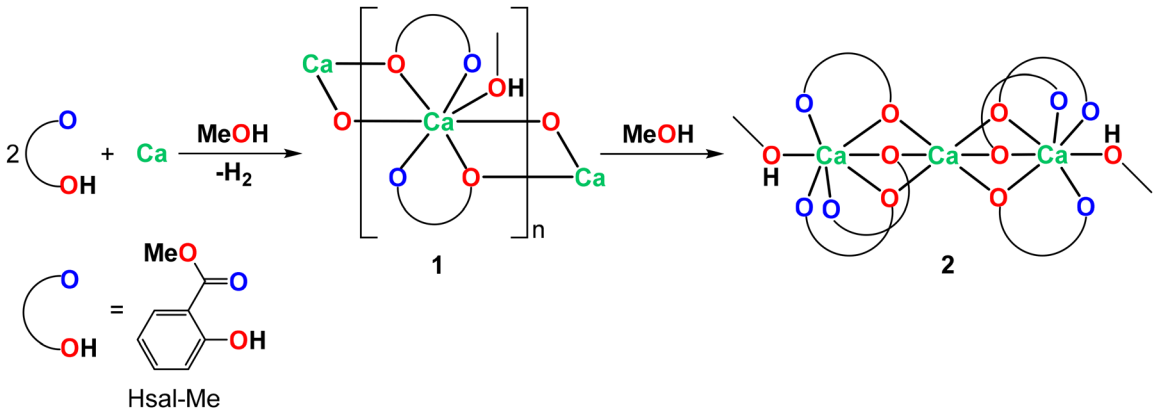

Scheme 1 Synthesis of **1** and **2**.

benzene-1,2-dioxydiacetate),[60,61] $[Ca_2(\mu\text{-}H_2O)(dhob)_2]_n$ ($dhob^{2-}$ = 3,5-dihydroxy-4-oxybenzoate),[62] $[Ca_2(dmob)_2(H_2O)_2]_n$ ($dmob^{2-}$ = 3,5-dimethoxy-4-oxybenzoate),[63] and $[Ca_2(dhtp)_2(H_2O)_x]_n$ ($dhtp^{2-}$ = 2,3-dihydroxyterephthalate, x = 0, 3; 2,5-dihydroxyterephthalate, x = 4).[64,65] Additional examples include $[Ca(3,5\text{-}NO_2sal)(H_2O)]_n$ ($3,5\text{-}NO_2sal^{2-}$ = 3,5-dinitrosalicylate),[66] and coordination polymers with phenolic sulfonate ligands, such as $[Ca(\mu\text{-}H_2O)(dhbds)]_n$ ($dhbds^{2-}$ = 4,6-dihydroxybenzene-1,3-disulfonate),[67] $[Ca_4(dobds)_2(H_2O)_{10}]_n$ ($dobds^{4-}$ = 4,6-dioxidobenzene-1,3-disulfonate), and $[Ca(L)_2(H_2O)_2]_n$ (L^- = 5-chloro-2-[2-(2-oxynaphthalen-1-yl)diazen-1-ium-1-yl]-4-methylbenzene-1-sulfonate).[68] Compound **1** crystallizes as a 1D coordination polymer from a concentrated methanolic solution. However, in the presence of excess MeOH, the polymer network is broken, leading to the formation of the trinuclear calcium complex $[Ca_3(sal\text{-}Me)_6(MeOH)_2]$ (**2**, 66%), which contains terminal methanol ligands as shown in Scheme 1. Calcium phenolates generally exhibit a tendency to form dinuclear or tetranuclear complexes, whereas the linear trinuclear core arrangement observed in **2** has previously been identified mainly in heterometallic rare-earth-calcium complexes of the type $[RE_2Ca(OAr)_8]$ (ArO^- = quinolin-8-olate; RE^{3+} = Sc^{3+}, Y^{3+}, Lu^{3+}, Yb^{3+}, Tm^{3+}, Ho^{3+}, Tb^{3+}, Gd^{3+}, Sm^{3+}, Nd^{3+}, Eu^{3+}, Er^{3+}).[69–72]

Notably, **1** and **2** represent the first structurally characterized calcium alkyl salicylates, which are commonly used as high-performance automotive lubricating oil additives.[73,74]

In **1**, the Ca1 atom is coordinated by two bidentate sal-Me ligands, two aryloxide oxygen atoms from two additional sal-Me ligands, and one MeOH molecule, adopting a capped trigonal prismatic geometry (Fig. 1). The same coordination geometry is observed for the external Ca1 and $Ca1^i$ atoms in **2**, which are coordinated by one MeOH and three sal-Me ligands (Fig. 2). In contrast, the central Ca2 atom in **2** is octahedrally coordinated by six aryloxide oxygen atoms (see ESI, Table S2†). The Ca–O bond lengths of 2.3593(10)–2.3928(10) Å in **1** and 2.3251(19)–2.3791(17) Å in **2** are slightly longer than those typically observed in calcium aryloxide structures.[75–78]

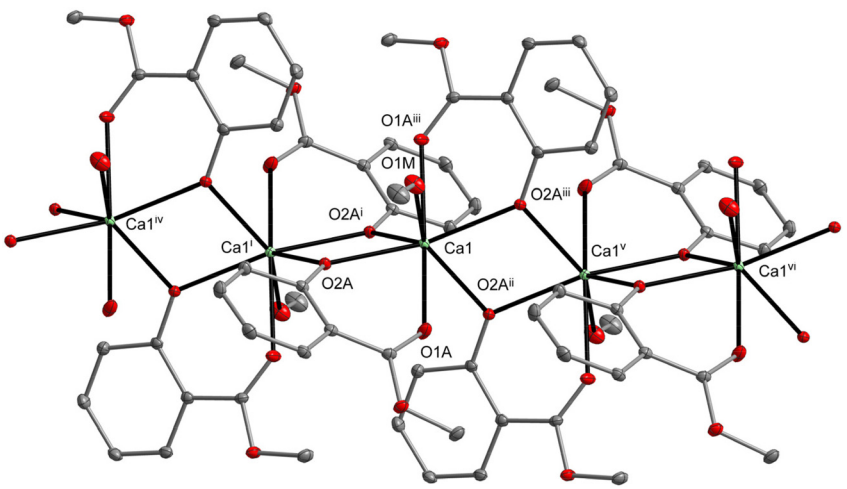

Fig. 1 The molecular structure of $[Ca(sal\text{-}Me)_2(MeOH)]_n$ (**1**). The displacement ellipsoids are drawn at the 25% probability level [symmetry code: (i) $-x+1, -y+1, -z+1$; (ii) $-1/2+x, y, -z+1$; (iii) $-x+1/2, -y+1, z$; (iv) $1+x, y, z$; (v) $-x, -y+1, -z+1$; (vi) $-1+x, y, z$]. Hydrogen atoms have been omitted for the sake of clarity.

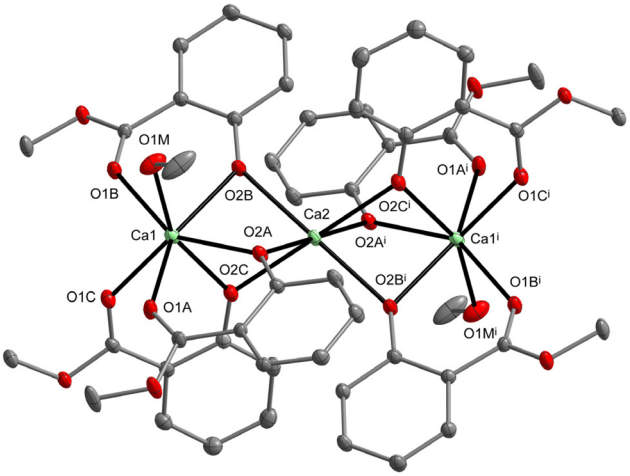

Fig. 2 The molecular structure of $[Ca_3(sal\text{-}Me)_6(MeOH)_2]$ (**2**). The displacement ellipsoids are drawn at the 25% probability level [symmetry code: (i) $-x + 1, -y + 1, -z + 1$]. Hydrogen atoms have been omitted for the sake of clarity.

Heterometallic calcium–alkali metal aryloxides form a small group of compounds, with only 13 examples of such coordination connections reported to date. Among these, the first group includes $[CaM'_6(\mu_3\text{-}OPh)_8(THF)_6]$ (M'^{+} = Li^+, Na^+), $[Ca_2Li_2(\mu\text{-}OPh)_6(dme)_4]$, and $[Ca_2Na_2(\mu_3\text{-}OPh)_2(\mu\text{-}OPh)_4(dme)_4]$, which feature vertex-sharing $\{CaM'_3O_4\}_2$ heterodicubane, a chain arrangement of double rhombi, or a double-open dicubane core structure, respectively.[46,47]

Another example consists of dinuclear or trinuclear Ca^{2+}–M'^{+} complexes with bulky 2,6-diphenylphenolato ligands, such as $[CaM'(OAr)_3]$ (M'^{+} = Na^+, K^+, Cs^+) and $[CaLi_2(OAr)_4]$. The final example, $[CaNa_2(L)_2(THF)_4]$, features a tridentate amido-iminophenolato ligand (L^{2-} = 2,4-di-*tert*-butyl-6-[(3-{[2,6-di-isopropylphenyl]imino}but-1-en-2-yl)amino]phenolato).[79]

Synthesizing heterobimetallic compounds of heavy alkaline earth and alkali metals is challenging due to their tendency to form mixtures of homometallic species and various mixed-metal aggregates. Fromm and colleagues demonstrated that the synthesis of heterometallic Ca^{2+}–M'^{+} compounds is not a straightforward reaction in which the final product structure can be easily controlled by adjusting reagent stoichiometry. For example, the reaction of CaI_2 with Na(OPh) in a 1 : 10 molar ratio results in the formation of $[CaNa_6(\mu_3\text{-}OPh)_8(THF)_6]$ in THF, whereas a THF/DME (2/1) solvent mixture yields $[Ca_2Na_2(\mu_3\text{-}OPh)_2(\mu\text{-}OPh)_4(dme)_4]$.[46] Moreover, ^{7}Li NMR studies revealed that $[CaLi_6(\mu_3\text{-}OPh)_8(THF)_6]$ in THF-d_8 undergoes disaggregation into $[Li_6(\mu_3\text{-}OPh)_6(THF)_6]$ and $[Ca_2Li_2(\mu_3\text{-}OPh)_2(\mu\text{-}OPh)_4(THF)_x]$, although the latter species has never been isolated in the solid state.[47] Another example, $[CaLi_2(OAr)_4]$, obtained from the reaction of Ca, ArOH, and Li (OAr) (3 : 2 : 1), demonstrates a different Ca : Li ratio than the initial reaction stoichiometry.[48]

In this study, the synthesis of heterometallic Ca^{2+}–M'^{+} compounds was achieved by reacting metallic calcium with Hsal-Me (1 : 3) in a THF/MeOH mixture, followed by the addition of 1 equivalent of M′ (M′ = Li, Na, K). The general synthetic routes, summarized in Scheme 2, led to the isolation of $[Ca_2Li_2(sal\text{-}Me)_6(THF)_2]$ (**3**, 57%), $[Ca_2Na_2(sal\text{-}Me)_6(MeOH)_4]$ (**4**,

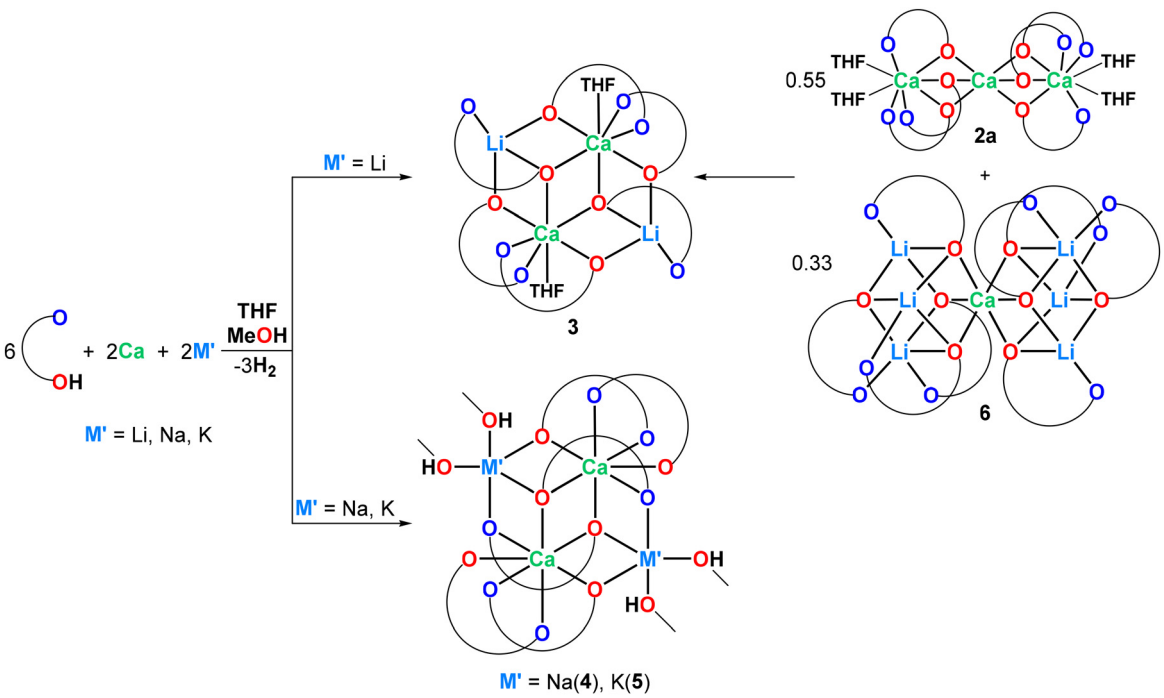

Scheme 2 Synthesis of heterometallic compounds **3**–**6**.

59%), and $[Ca_2K_2(sal\text{-}Me)_6(MeOH)_4]$ (**5**, 69%). Compounds **3–5** share the same structural motif as the recently reported by our group alkali metal–magnesium aryloxides $[Mg_2M'_2(sal\text{-}Me)_6(THF)_x]$ (M'^{+} = Li^+, Na^+, K^+; x = 0, 2, 4).[80]

Compound **3** is isostructural with the previously published $[M_2Li_2(sal\text{-}Me)_6]$ (M^{2+} = Mg^{2+}, Zn^{2+}), in which the common face-sharing vertices of the central core are occupied by M^{2+} ions, while the external vertices are occupied by Li^+ ions (Fig. 3). Similarly, in **4** and **5**, the M'^{+} ions are positioned at the external vertices, demonstrating a reversed metal atom arrangement in the tetranuclear units compared with $[Mg_2M'_2(sal\text{-}Me)_6(THF)_x]$ (M'^{+} = Na^+, K^+) as shown in Fig. 4. A continuous shape measure (CShM) analysis of the coordination geometries in **3** and **4** revealed that Ca^{2+} ions are surrounded by seven oxygen donor atoms, forming capped trigonal prisms (ESI, Table S2†). The external Li^+ or Na^+ ions adopt axially vacant trigonal bipyramidal or vacant octahedral geometries, respectively (ESI, Table S2†). For the X-ray diffraction study, compound **3** was isolated as cocrystals with the general

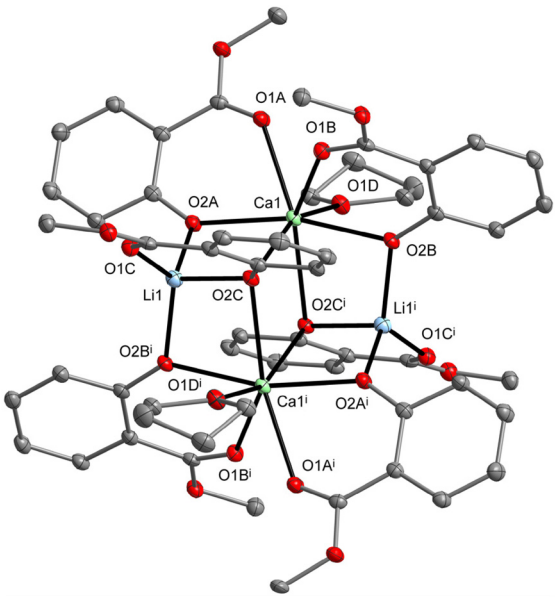

Fig. 3 The molecular structure of $[Ca_2Li_2(sal\text{-}Me)_6(THF)_2]$ (**3**) in cocrystal $[Ca_2Li_2(sal\text{-}Me)_6(THF)_2]\cdot[Ca_3(sal\text{-}Me)_6(THF)_4]$ (**3·2a**). The displacement ellipsoids are drawn at the 25% probability level [symmetry code: (i) $-x+1, -y, -z+2$]. Hydrogen atoms have been omitted for the sake of clarity.

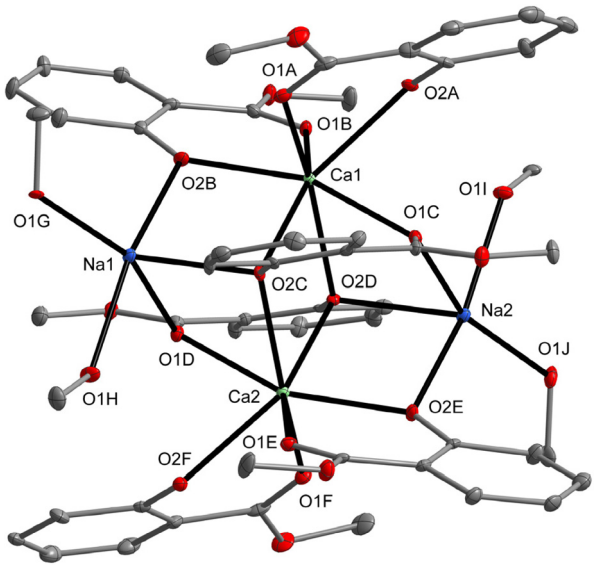

Fig. 4 The molecular structure of $[Ca_2Na_2(sal\text{-}Me)_6(MeOH)_4]$ (**4**). The displacement ellipsoids are drawn at the 25% probability level. Hydrogen atoms have been omitted for the sake of clarity.

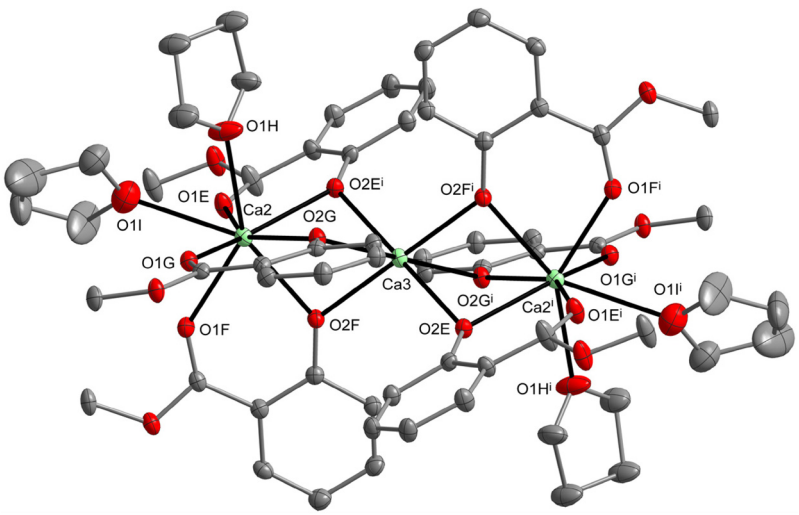

Fig. 5 The molecular structure of $[Ca_3(sal\text{-}Me)_6(THF)_4]$ (**2a**) in cocrystal $[Ca_2Li_2(sal\text{-}Me)_6(THF)_2]\cdot[Ca_3(sal\text{-}Me)_6(THF)_4]$ (**3·2a**). The displacement ellipsoids are drawn at the 25% probability level [symmetry code: (i) $-x, -y, -z+1$]. Hydrogen atoms have been omitted for the sake of clarity.

formula $[Ca_2Li_2(sal\text{-}Me)_6(THF)_2]\cdot[Ca_3(sal\text{-}Me)_6(THF)_4]$ (**3·2a**, 45%), containing additional $[Ca_3(sal\text{-}Me)_6(THF)_4]$ species (**2a**) (Fig. 5).

The presence of excess calcium ions in **3·2a** suggests a non-stoichiometric reaction between these two metallic species, leading to the formation of an additional Li-rich compound, $[CaLi_6(sal\text{-}Me)_8]$ (**6**, 78%). In **6**, the six-coordinate Ca1 atom adopts an octahedral geometry, while the Li^+ ions exhibit four- and five-fold coordination, forming either axially vacant trigonal bipyramid (Li1) or trigonal bipyramid (Li2 and Li3) (Fig. 6; ESI, Table S2†).

Further detailed analysis of the reaction pathway revealed that **6**, based on a vertex-sharing $\{CaLi_3O_4\}_2$ heterodicubane, forms as the main product alongside **2a** in the initial reaction step. Subsequent reaction of **6** with **2a** in a concentrated THF solution leads to the formation of **3**, as shown in Scheme 2.

Analogous studies on intermediate products isolated from the reaction of Ca and Na with Hsal-Me (1 : 1 : 3), conducted in an EtOH/toluene solution, resulted in the formation of the heptanuclear sodium-rich aryloxide $[Ca_3Na_4(sal\text{-}Et)_{10}(Hsal\text{-}Et)_2]$ (**7**, 72%) as shown in Fig. 7. Structurally, **7** can be considered as two Ca1-sharing double-open dicubanes. The central Ca1 atom, chelated by four sal-Et ligands, adopts a square antiprismatic geometry, while Ca2 and Ca3 are octahedrally coordinated by six oxygen donor atoms from four sal-

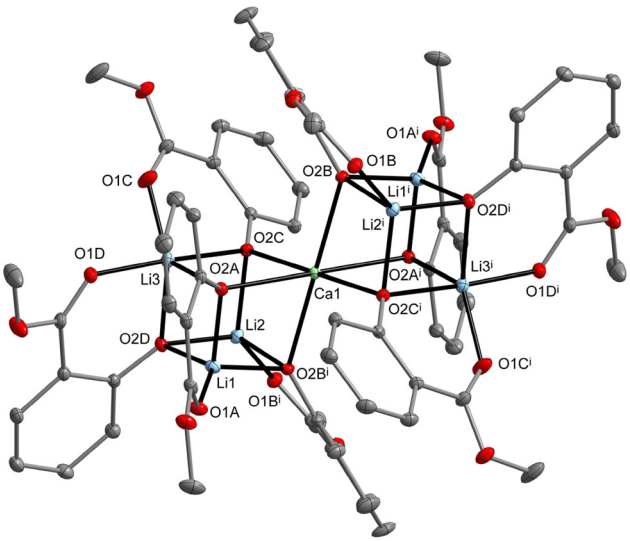

Fig. 6 The molecular structure of $[CaLi_6(sal\text{-}Me)_8]$ (**6**). The displacement ellipsoids are drawn at the 25% probability level [symmetry code: (i) $-x + 1, -y + 1, -z + 1$]. Hydrogen atoms have been omitted for the sake of clarity.

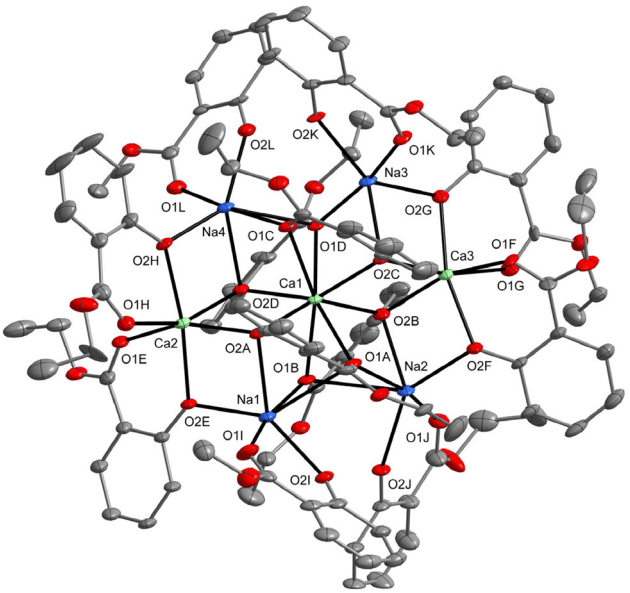

Fig. 7 The molecular structure of $[Ca_3Na_4(sal\text{-}Et)_{10}(Hsal\text{-}Et)_2]$ (**7**). The displacement ellipsoids are drawn at the 25% probability level. Hydrogen atoms have been omitted for the sake of clarity.

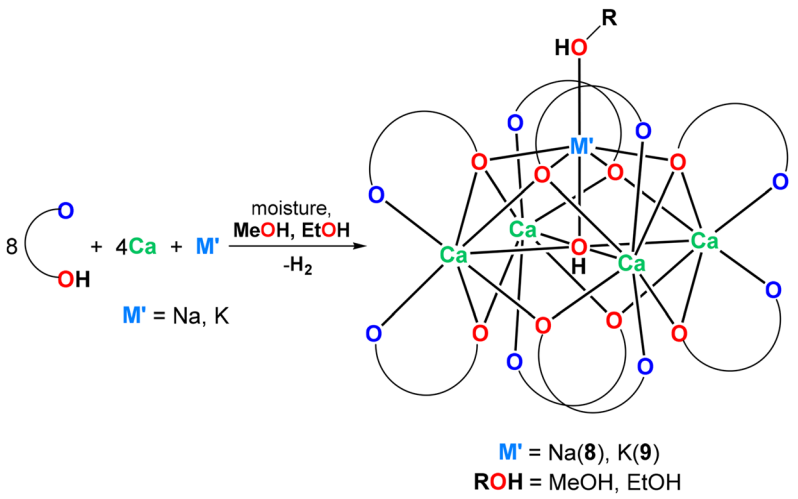

Scheme 3 Synthesis of heterometallic compounds **8–9**.

Et ligands. The Na^+ ions, surrounded by six oxygen donors, adopt highly distorted trigonal prismatic (Na1) or octahedral (Na2–Na4) geometries. Furthermore, the presence of a linear trinuclear $\{Ca_3O_4\}$ unit in **7**, capped by four Na(sal-Et) species, suggests a possible transformation pathway from **2** or **2a** into **4**. The molecular structures of the isolated intermediates **6** and **7** expand the existing group of Ca^{2+}–M'^{+} compounds, significantly enhancing our understanding of their chemistry, reactivity, and solid-state aggregation phenomena.

The Ca–O bond distances in compounds **3**–**7** (2.291(2)–2.466(2) Å in **3**, 2.288(5)–2.491(5) Å in **4**, 2.3404(11)–2.3630(11) Å in **6**, and 2.209(14)–2.539(4) Å in **7**) are comparable and align well with previously reported parameters for calcium complexes containing O,O′-chelating ligands.[81–84] The Li–O bond distances in **3** (1.876(5)–1.934(6) Å) are consistent with those reported for $[Li_6(sal\text{-}Me)_6]$, [Li(sal-Me)(Hsal-Me)], and $[Li(sal\text{-}Me)(MeOH)_2]$.[85] In contrast, the Li–O distances in **6** (1.846(3)–2.088(3) Å) resemble those found in tetranuclear $[AlLi_3(sal\text{-}Me)_6]$.[86] The Na–O bond distances in **4** (2.267(6)–2.387(6) Å) fall within the expected range for this type of coordination, as observed in $[Na_2Zn_2(sal\text{-}Me)_6]_n$,[80] and $[NaEr(sal\text{-}H)_3]_n$.[87] The significantly elongated Na–O bonds in **7** (2.845(4)–2.886(4) Å) further support the hypothesis of Na(sal-Et) species aggregation on the trinuclear $\{Ca_3(sal\text{-}Et)_6\}$ motif observed in **2** or **2a**.

The final group of heterometallic Ca^{2+}–M'^{+} aryloxides includes $[Ca_4Na(\mu_5\text{-}OH)(sal\text{-}Et)_8(MeOH)]$ (**8**, 62%) and $[Ca_4K(\mu_5\text{-}OH)(sal\text{-}Et)_8(EtOH)]$ (**9**, 74%), obtained from the reaction of 8 equivalents of Hsal-Me with 4 equivalents of Ca and 1 equivalent of Na/K in ROH/THF solution, followed by exposure to atmospheric moisture or the deliberate addition of water (Scheme 3). Crystallographic analysis of **8** and **9** reveals Na^+/K^+ ions coordinated by MeOH/EtOH ligands, disordered over two positions at opposite ends of the pyramidal base formed by four Ca atoms bridged by OH group (Fig. 8 and 9; ESI, Fig. S1 and S2†).

The pentanuclear cores of **8** and **9** (Fig. 8 and 9) resemble those in heterometallic Ca^{2+}/Eu^{2+}–Li^+ μ_5-hydroxo-alkoxides of the general formula $[MLi_4(\mu_5\text{-}OH)(\mu_3\text{-}O^tBu)_4(THF)_4I]$ (M^{2+} = Ca^{2+}, Eu^{2+}).[46] The number of known pentanuclear homometallic alkaline-earth μ_5-hydroxo-alkoxides/aryloxides is limited to only four examples: $[Ba_5(\mu_5\text{-}OH)(\mu_3\text{-}OR)_4(\mu\text{-}OR)_4(OR)(H_2O)(THF)_4]$ (RO^- = hexafluoroisopropoxo),[88] $[Ba_5(\mu_5\text{-}OH)(\mu_3\text{-}OR)_4(\mu\text{-}H_2O)_3(OR)_5]$ (RO^- = 2,2,6,6-tetramethyl-3,5-heptanedionato),[89] $[Ba_5(\mu_5\text{-}OH)(\mu_3\text{-}OAr)_4(\mu\text{-}OAr)_4(OAr)(THF)_5]$ (ArO^- = 3,5-di-*t*-butylphenolato),[90] and $[Ba_5(\mu_5\text{-}O)(\mu_3\text{-}OPh)_4(\mu\text{-}OPh)_4(PhOH)(THF)_8]$.[91]

In isostructural compounds **8** and **9**, the capped trigonal prismatic coordination geometry around Ca^{2+} ions exhibits comparable deformations, as indicated by the CShM parameters *S*(CTPR-7), which range from 1.012 to 1.386 for **8** and from 0.752 to 1.586 for **9** (ESI, Table S2†). Within the group of alkali metal ion octahedra, the smaller geometric deformation was observed for Na^+-containing polyhedra (*S*(Oh) = 3.570–3.547 for Na1/Na2 and 6.771–6.919 for K1/K2). The coordination environments of Ca^{2+} in **8** and **9**, along with Ca–O(sal-Et) bond distances of 2.331(4)–2.402(4) Å for **8** and 2.327(2)–2.411(2) Å for **9**, are similar to those reported for **1** and **2**.

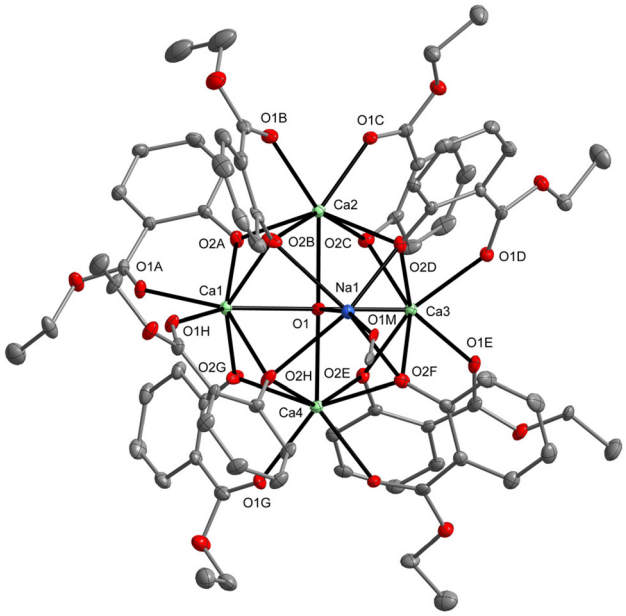

Fig. 8 The molecular structure of $[Ca_4Na(\mu_5\text{-}OH)(sal\text{-}Et)_8(MeOH)]$ (**8**). The displacement ellipsoids are drawn at the 25% probability level. Hydrogen atoms and the second disordered component of Na atom and MeOH ligand have been omitted for the sake of clarity.

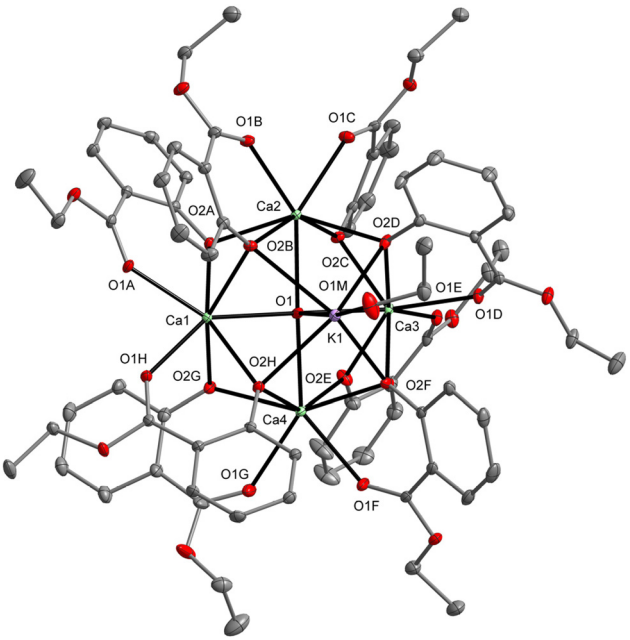

Fig. 9 The molecular structure of $[Ca_4K(\mu_5\text{-}OH)(sal\text{-}Et)_8(EtOH)]$ (**9**). The displacement ellipsoids are drawn at the 25% probability level. Hydrogen atoms and the second disordered component of K atom and EtOH ligand have been omitted for the sake of clarity.

Likewise, the Ca–OH bond lengths of 2.391(3)–2.429(3) Å for **8** and 2.391(2)–2.402(2) Å for **9** are elongated compared to those observed in $[Ca_4(\mu_3\text{-}OH)_2(OAr)_6(en)_4]$ (ArO^- = 2,4,6-trimethylphenolato)[92] and $[Ca_4(\mu_3\text{-}OH)_2(OAr)_6(THF)_6]$ (ArO^- = 2-isopropylphenolato).[21] The Na–O(sal-Et) bond lengths of 2.438

(4)–2.633(5) Å, Na–OH bond lengths of 2.336(5)–2.363(5) Å, K–O(sal-Et) bond lengths of 2.694(2)–2.898(3) Å, and K–OH bond lengths of 2.816(3)–2.855(3) Å are significantly longer than those typically reported for alkali metal aryloxides. However, they are similar to bond lengths found in the structures of homometallic or heterometallic alkali metal salicylic acid derivatives, such as $[Mg_2M'_2(sal\text{-}Me)_6(THF)_x]$ (for $M'^{+} = Na^+$, K^+, and x = 2, 4),[80] $[Mg_4Na_2(sal\text{-}Me)_6(sal)_2(THF)_4]$, $[Mg_6Na_4Al(sal\text{-}Me)_{13}(OH)_6(Hsal\text{-}Me)(THF)_{0.5}(H_2O)_{0.5}]$, $[MgK(sal\text{-}Et)_3]_n$,[93] and $[M'_2(\mu\text{-}H_2O)_2(dhb)_6]$ (for $M'^{+} = Na^+$, K^+; dhb^{2-} = 2,4-dihydroxybenzoato)[94]

Compounds **1–9** were isolated as crystalline materials with good solubility in aromatic and ether solvents. They were characterized using analytical methods, FTIR-ATR, and NMR spectroscopy (ESI, Fig. S3–S31†). The ^{1}H-DOSY NMR study of **1–8** in THF-d_8 was conducted to investigate the nature of homometallic and heterometallic calcium aryloxides in solution (ESI, Fig. S32–S42, Tables S3 and S4†). Dissolution of **1** in THF-d_8 led to the formation of $[Ca_3(sal\text{-}Me)_6(THF)_4]$ (**2a**) and higher aggregates of $[Ca(sal\text{-}Me)_2]_x$ (where x = 8), as verified by ^{1}H-DOSY NMR measurements (Fig. S32, S33 and Table S3†). In compounds **4** and **5**, donor MeOH ligands were removed from the alkali metal coordination sphere *via* vacuum drying before NMR measurements. Subsequent dissolution in THF-d_8 resulted in the coordination of THF ligands. ^{1}H-DOSY NMR analysis of **3–5** confirmed the presence of tetranuclear species in solution, with estimated formula weights and hydrodynamic radii (**3**: FW = 1074 g mol^{-1}, rH = 8.79 Å; **4**: FW = 1275 g mol^{-1}, rH = 9.31 Å; **5**: FW = 1158 g mol^{-1}, rH = 9.02 Å), which correlate well with data from X-ray structures (ESI, Fig. S34–S39, Tables S3 and S4†). Additionally, compounds **6–8** retain their structural integrity in solution (ESI, Fig. S40–S42†).

Catalytic applications of homometallic and heterometallic calcium aryloxides in chemical recycling of PA6

The alcoholysis reactions using MeOH as a reagent and homometallic and heterometallic aryloxides as catalysts were studied as a chemical recycling method for post-consumer nylon-6 waste. Previous studies on PA6 alcoholysis have demonstrated that depolymerization of PA6 with supercritical MeOH at 300–370 °C produces CL, *N*-methylcaprolactam, methyl 6-hydroxycaproate, methyl 5-hexenoate, and methyl 6-(*N*,*N*-dimethylamino)caproate, with total yields ranging from 77% to 81% (ESI, section: Chemical recycling of PA6†).[95] A similar approach using supercritical primary alcohols (MeOH, EtOH, ^{n}PrOH, ^{n}BuOH) enables the recovery of 14–47% CL at 370 °C after 1.5 h (PA6/ROH = 1/13.33 wt), with yields increasing as the alkyl chain length of the alcohol increases.[96]

Our studies utilized commercially available zip ties and mowing lines as sources of nylon-6 resins for catalytic reactions. Before the catalytic investigation, both plastic materials were analyzed using TGA-DSC to determine their phase transition temperatures and thermal stability. The polymer demonstrated excellent thermal stability up to 375 °C, with weight loss not exceeding 10%. The maximum degradation temperature was 438.5 °C for PA6 (mowing line) and 427.0 °C for PA6 (zip tie) (Fig. 10a). During the first heating scan, both materials exhibited a single endothermic peak corresponding to the melting of α-form PA6 crystals at 219.9 °C and 222.8 °C, respectively (Fig. 10b).

Typical reactions were conducted under solvothermal conditions at 200–240 °C for 8 hours in 25 mL PTFE-lined hydrothermal reactors, using compounds **2–9** as catalysts with a stoichiometry of [PA6]/[MeOH]/[Ca] = 1/50/0.05. The resulting products were identified using FTIR-ATR spectroscopy, ESI-MS, and ^{1}H and ^{13}C NMR spectroscopy. The progress of the alcoholysis reactions and the catalytic activity of compounds **2–9** were monitored over time by ^{1}H NMR spectroscopy. The results showed that 5–92% of the PA6 was consumed, yielding a liquid consisting of oligomers of 6-aminocaproic acid and low molecular weight organic products (Fig. 11).

The FTIR–ATR spectrum of virgin PA6, presented in Fig. 12, exhibits strong N–H stretching vibrations at 3400–3200 cm^{-1} (amide A), C═O stretching at ~1635 cm^{-1} (amide I), and N–H bending coupled with C–N stretching at ~1539 cm^{-1} (amide II). Additionally, a combination of C–N stretching and N–H bending vibrations is observed at 1260 cm^{-1} (amide III).

The aliphatic chain contributes C–H stretching at ~2930 cm^{-1} and bending at 1462 cm^{-1}, along with additional C–H bending adjacent to N–H at 1436 cm^{-1}. Scissoring and

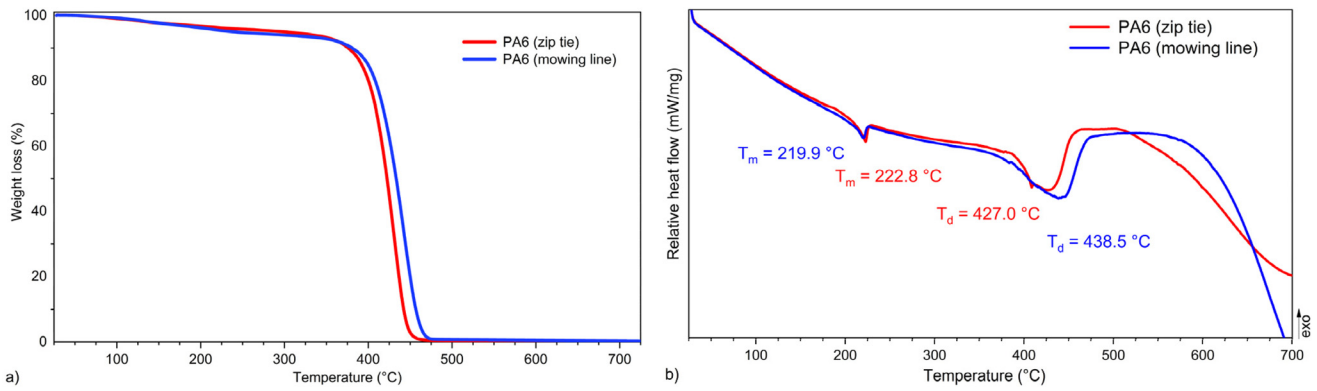

Fig. 10 TGA (a) and DSC (b) thermograms of PA6 zip ties and mowing lines investigated in alcoholysis reactions.

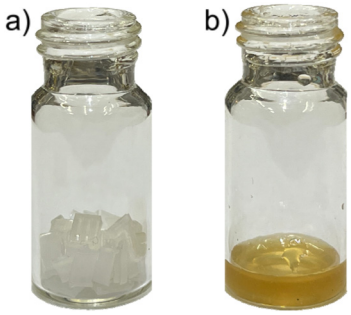

Fig. 11 The PA6 waste used in the chemical recycling process (a) and the liquid mixture of organic products obtained from the alcoholysis reaction at 240 °C (b).

twisting vibrations of CH_2 groups appear at 1419 and 1371 cm^{-1}, respectively, while a twisting vibration associated with the amide III band is observed at 1238 cm^{-1}. Other characteristic vibrations include CH_2 wagging at 1202 cm^{-1} and C–N skeletal vibrations at 1170 and 1118 cm^{-1}. Peaks at 1027, 974, 929, and 830 cm^{-1} indicate the crystalline α-phase of PA6, with a signal at 726 cm^{-1} corresponding to CH_2 wagging vibrations. N–H bending vibrations appear at 684 cm^{-1}, while C=O bending is observed at 577 cm^{-1}. The spectrum is completed by a C–C skeletal vibration at 519 cm^{-1}.

Comparison of FTIR–ATR spectra of PA6 and its methanolysis products (Fig. 12; ESI, Fig. S43†) highlights the breakdown of amide linkages and the formation of low molecular weight esters, hydroxyesters, cyclic lactams, or linear oligomers of 6-aminocaproic acid, providing insights into the chemical recycling process. The FTIR–ATR spectrum of the sample depolymerized at 220 °C after 8 hours primarily consists of methanol-soluble oligomers of 6-aminocaproic acid, as evidenced by sharp and well-defined amide A and I–III bands.

The spectrum of the sample depolymerized at 240 °C after 61 hours reveals a broad O–H stretching vibration at 3302 cm^{-1}, a sharp C=O stretching vibration at 1736 cm^{-1}, and scissoring vibrations of the methyl ester group at 1437 cm^{-1}, confirming the formation of methyl esters of carboxylic or hydroxycarboxylic acids. The presence of CL in the reaction mixture is well recognized by the appearance of C–N stretching vibration at 1437 cm^{-1} as well as C–H and N–H rocking vibrations at 577 and 484 cm^{-1}, respectively. The amide II band is shifted to higher wavenumbers, demonstrating the changes in the amide bond environment caused by polymer chain cutting.

ESI-MS analysis of the previously examined samples confirmed the degradation of PA6 into a liquid mixture containing oligomers of 6-aminocaproic acid, X–$[HN(CH_2)_5CO]_n$–$O(CH_3/H)$, capped by four distinct end groups (X). These include 5-hexenoyl (**A** and **B** series), 6-methoxyhexanoyl (**C** series),

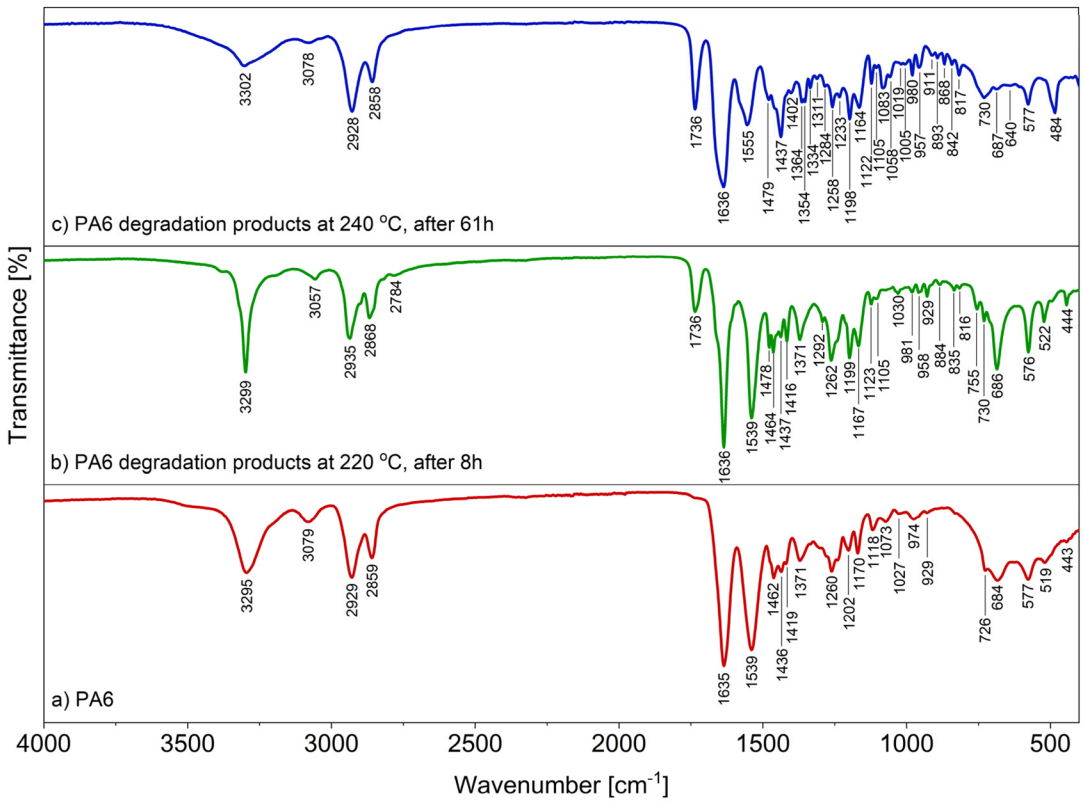

Fig. 12 Comparison of FTIR-ATR spectra of virgin PA6 (a) and liquid organic products obtained from PA6 methanolysis using **2** as a catalyst after 8 h at 220 °C (b) and 61 h at 240 °C (c).

6-hydroxyhexanoyl (**D** series), and 6-(dimethylamino)hexanoyl (**E** series), as well as cyclic oligomers (**F** series) (Fig. 13 and ESI, Fig. S44–S49†). When the reaction temperature was increased to 240 °C and the reaction time extended from 8 to 61 hours, an increased intensity of low molecular weight products, such as CL and its *N*-methyl or methanolyzed derivative, $H_2N(CH_2)_5(CO)OCH_3$, was observed (Fig. 13).

The ^{1}H NMR spectrum of the liquid products obtained from PA6 methanolysis after 61 h, supported by ^{1}H–^{1}H COSY and ^{1}H–^{13}C HSQC analyses, revealed the formation of a mixture of seven distinct compounds (Fig. 14 and 15; ESI, Fig. S50†). As the reaction progressed, PA6 degraded into low molecular weight oligomers (**I**) and caprolactam (**II**). Subsequently, the NH group in **II**, along with the NH_2 group in $H_2N(CH_2)_5(CO)OCH_3$, underwent alkylation by MeOH, forming *N*-methylcaprolactam (**III**) and methyl 6-(*N*,*N*-dimethylamino)caproate (**IV**). Under prolonged heating, **III** and **IV** were further converted into methyl 6-hydroxycaproate (**V**), methyl 6-methoxycaproate (**VI**), and methyl 5-hexenoate (**VII**), with **VI** being formed through direct etherification of

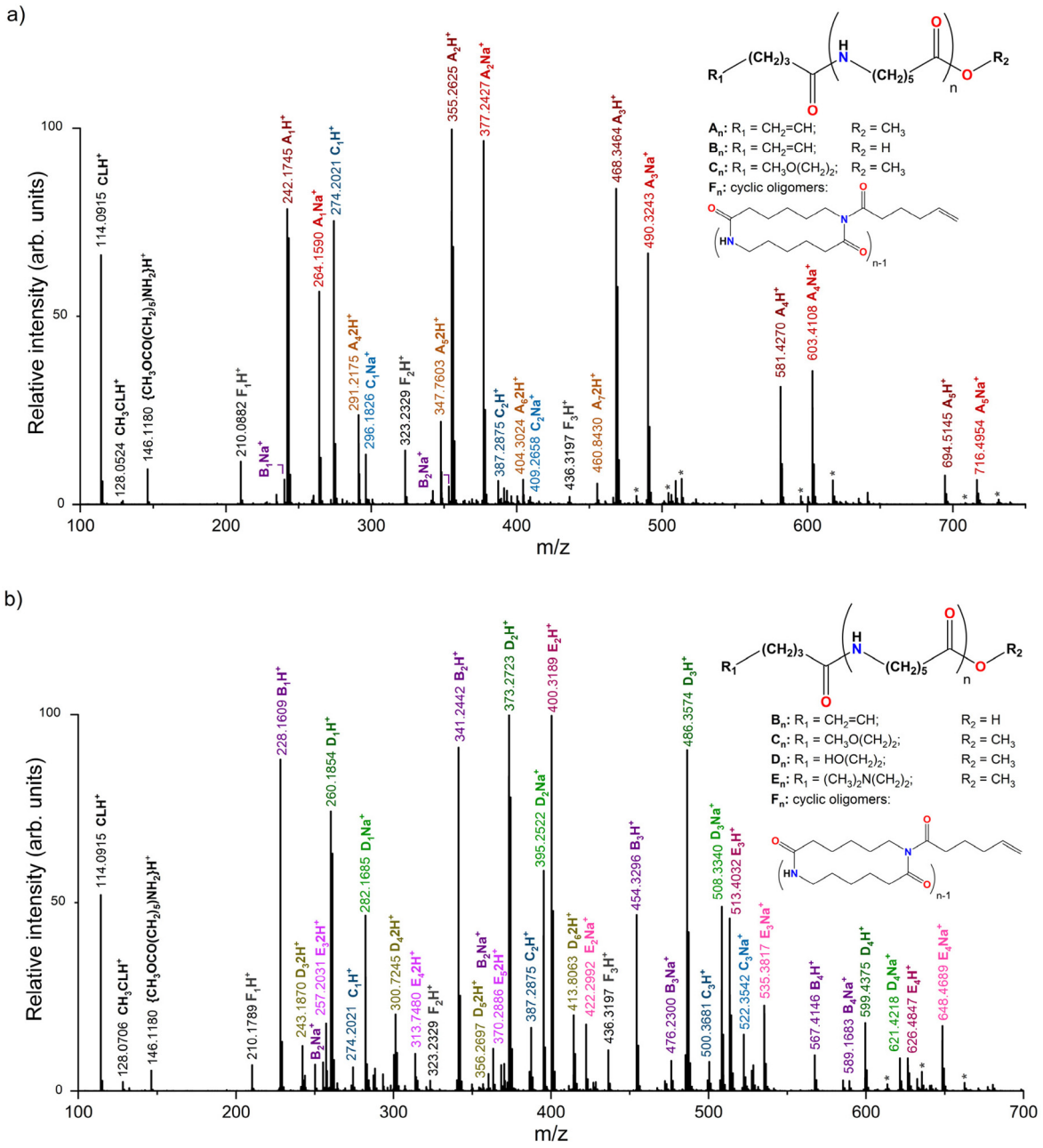

Fig. 13 Comparison of ESI-MS spectra of liquid organic products obtained from PA6 methanolysis at 240 °C using **2** as a catalyst after 61 h (a and b). ESI-MS spectra were recorded for fractions collected from 3.79 to 4.01 min (a) and 3.33 to 3.69 min (b). The * symbol denotes a series containing one 6-(methylamino)hexanoate unit instead of 6-aminohexanoate.

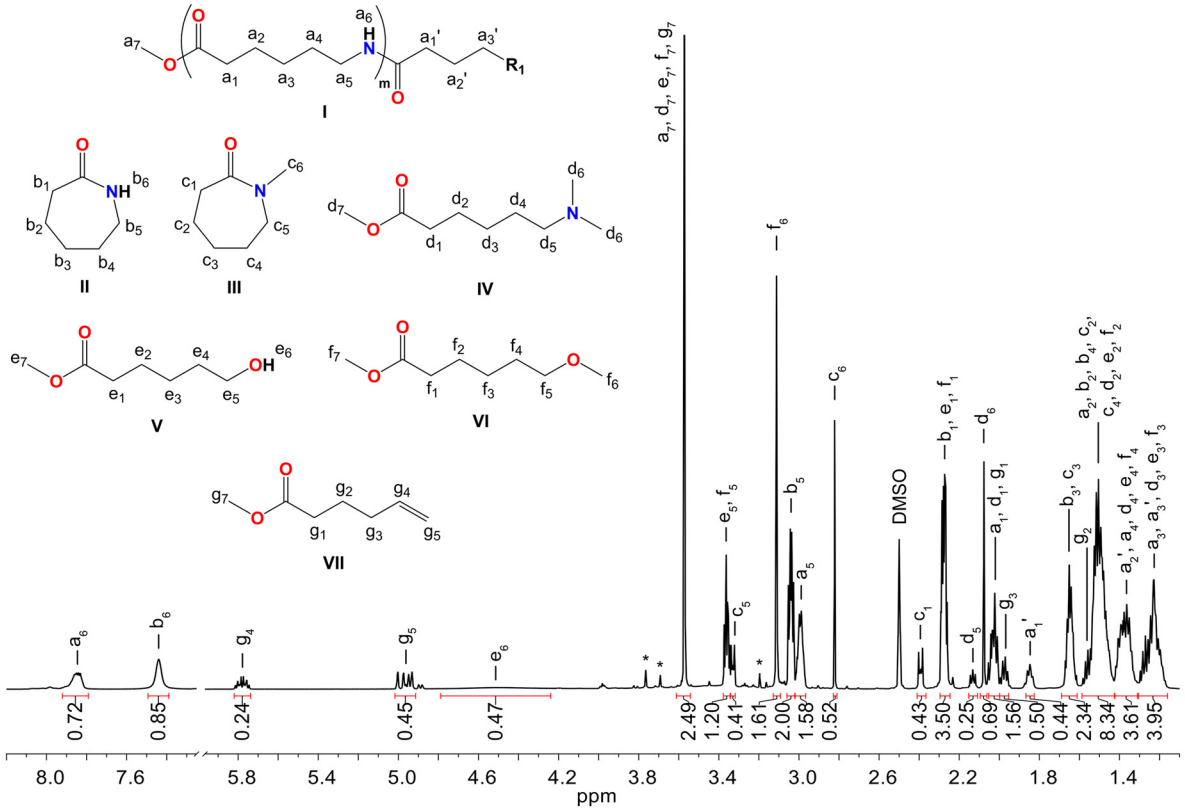

Fig. 14 ^{1}H NMR spectrum of liquid organic products obtained from PA6 methanolysis at 240 °C after 61 h using **2** as a catalyst. * – Traces of unidentified products and PA6 additives.

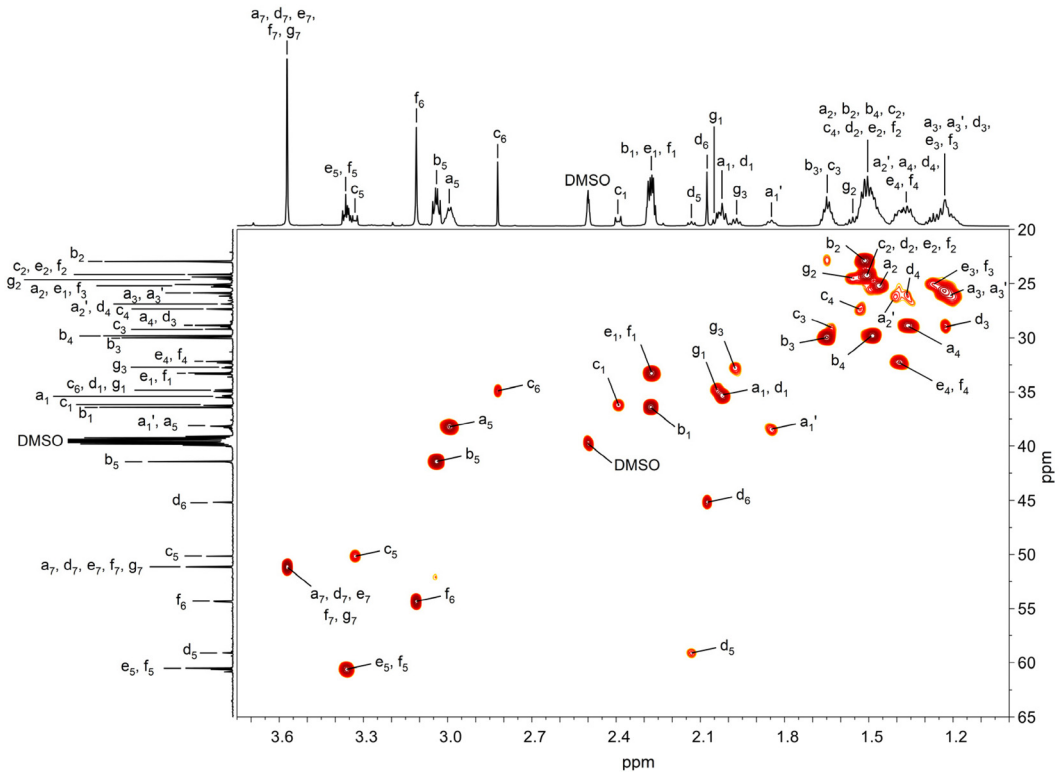

Fig. 15 ^{1}H–^{13}C HSQC NMR spectrum of liquid organic products obtained from PA6 methanolysis using **2** as a catalyst after 61 h at 240 °C.

V. The overall pathway for the chemical recycling of PA6 is summarized in Scheme 4.

The comparison of ^{1}H NMR spectra of the products obtained from PA6 methanolysis using **2** as a catalyst after 8 h at 220 °C and after 8 or 61 h at 240 °C (Fig. 16; Fig. S50–S52†) revealed that lower reaction temperatures and shorter reaction times primarily favor the degradation of PA6 into oligomers (**I**). As both reaction time and temperature increase, the intensity of signals corresponding to products **II–VII** also increases. For instance, at 240 °C, the conversion of PA6 into **I**/**II**/**III**/**IV**/**V**/**VI**/**VII** was observed as 34%/12%/1%/7%/12%/4%/1% after 8 h and 27%/34%/6%/4%/3%/18%/8% after 61 h. An important economic consideration in these studies is the ability to achieve rapid PA6 decomposition.

After identifying a suitable system for the chemical recycling of PA6 to compounds **I–VII**, we investigated a broad range of catalysts to achieve high product yields under mild reaction conditions, including low pressure, low temperature, and short reaction times. First, we examined the catalytic activities of compounds **2–9** in PA6 methanolysis under standard conditions: [PA6]/[MeOH]/[Ca] = 1/50/0.05 at 200–240 °C for 8 h. The results indicate that PA6 conversion typically ranges from 5% to 20% at 200 °C, except for catalyst **6**, which achieves 61% conversion (ESI, Table S5†). The high reactivity of **6** in this reaction significantly surpasses that of alkali metal aryloxides $[M'_6(sal\text{-}Me)_6]$ (where M'^{+} = Li^+ (**10**), Na^+ (**11**), K^+ (**12**)), divalent metal aryloxides **2**, $[Mg_2(sal\text{-}Et)_4(EtOH)_2]$ (**13**) and $[Zn_4(sal\text{-}Me)_8]$ (**14**), as well as heterometallic aryloxides **3–5**, **7–9**, $[M_2M'_2(sal\text{-}Me)_6(THF)_x]$ (where M^{2+} = Mg^{2+} and M'^{+} = Li^+ (**15**), Na^+ (**16**), K^+ (**17**); or M^{2+} = Zn^{2+} and M'^{+} = Li^+ (**18**), Na^+ (**19**), K^+ (**20**); with x = 0, 2, 4), and $[Mg_4Na_2(sal\text{-}Me)_6(sal)_2(THF)_4]$ (**21**). Scheme 5 summarizes the homometallic and heterometallic aryloxides (**10–21**) investigated in PA6 alcoholysis.

In addition to compound **6**, catalysts **10** (41%), **14** (39%), **17** (39%), and **20** (50%) also exhibited high activity at 200 °C. When the reaction temperature was increased to 220 °C, good catalytic performance was observed for compounds **3**, **10**, and **18–20**, with PA6 conversion values ranging from 60% to 69% (ESI, Table S5†). However, as before, the highest conversion (84%) was achieved with catalyst **6** (Fig. 17).

At 240 °C, within the heterometallic double-opened tetranuclear catalyst group, compounds **15–20** demonstrated comparable and significantly higher activity (86%–98%) than catalysts **3–5** (81%–92%). The highest catalytic activity at 240 °C, with polymer conversion exceeding 90%, was observed for catalysts **3** (92%), **6** (93%), **7** (93%), **15** (97%), **16** (98%), **18** (96%), and **19** (97%).

For the catalysts mentioned above, which yielded similar PA6 conversion values, the composition of individual products in the resulting mixture was also very similar (ESI, Table S5†). The product distribution was within the following ranges: **I** (35%–44%), **II** (18%–24%), **III** (2%–3%), **IV** (9%–10%), **V** (10%–16%), **VI** (5%–10%), and **VII** (3%–4%), as shown in Fig. 18 (ESI, Table S5†). A comparison of these results with those from catalyst-free reactions reveals an exceptionally high PA6 conversion, reaching 29% at 220 °C and 60% at 240 °C. This high conversion is attributed to the significantly higher autogenous pressures of the reactants compared to reactions performed with catalysts.

When the reaction time was extended from 8 to 48 h at 220 °C, the overall PA6 conversion ranged from 92% to 100%, yielding individual product distributions as follows: **I** (26%–35%), **II** (21%–30%), **III** (3%–6%), **IV** (5%–8%), **V** (1%–18%), **VI** (9%–25%), and **VII** (4%–8%) (ESI, Table S6†). The results indicate that prolonging the reaction time generally led to either a slight decrease or minimal increase in the yield of **I**, a 2- to

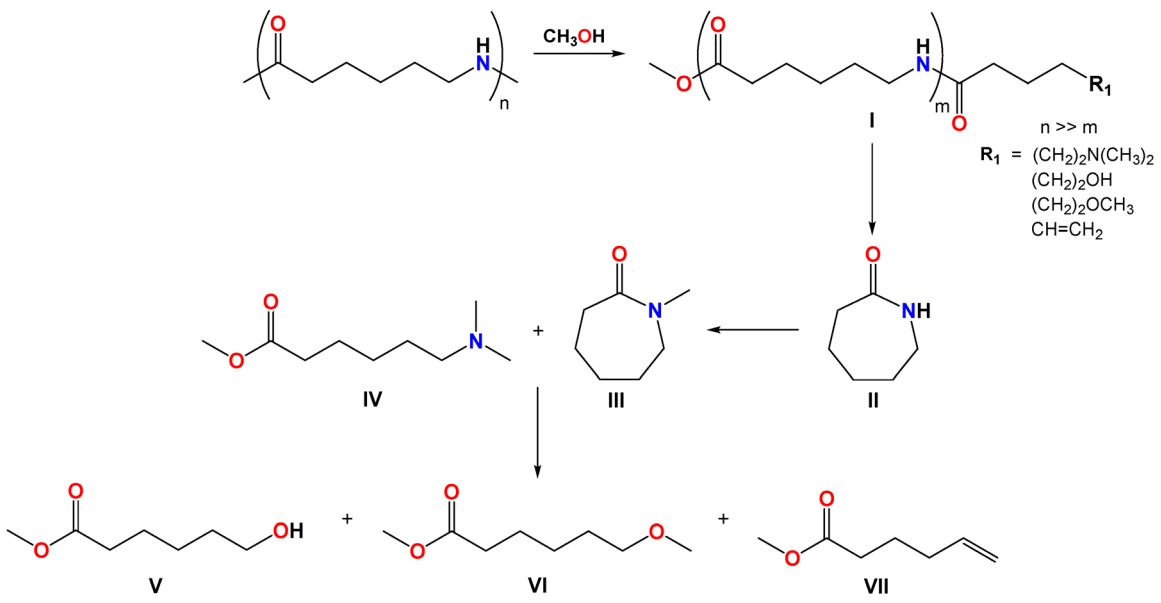

Scheme 4 The general route for the methanolysis of PA6.

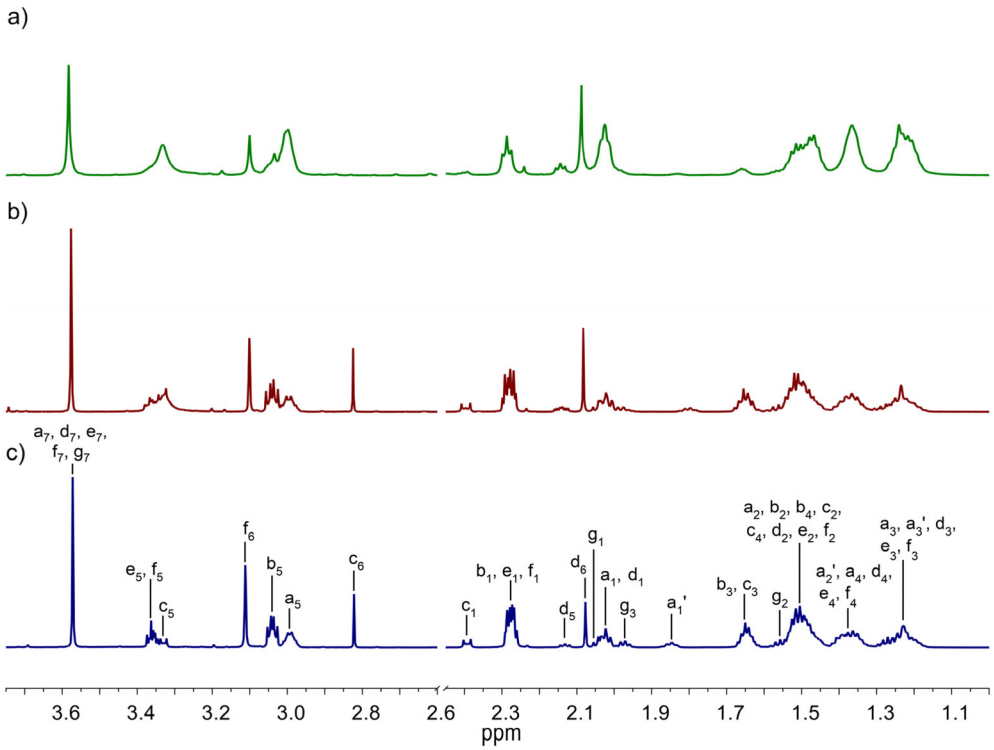

Fig. 16 Comparison of ^{1}H NMR spectra of liquid organic products obtained from PA6 methanolysis using **2** as a catalyst after 8 h at 220 °C (a), and after 8 h (b) or 61 h (c) at 240 °C.

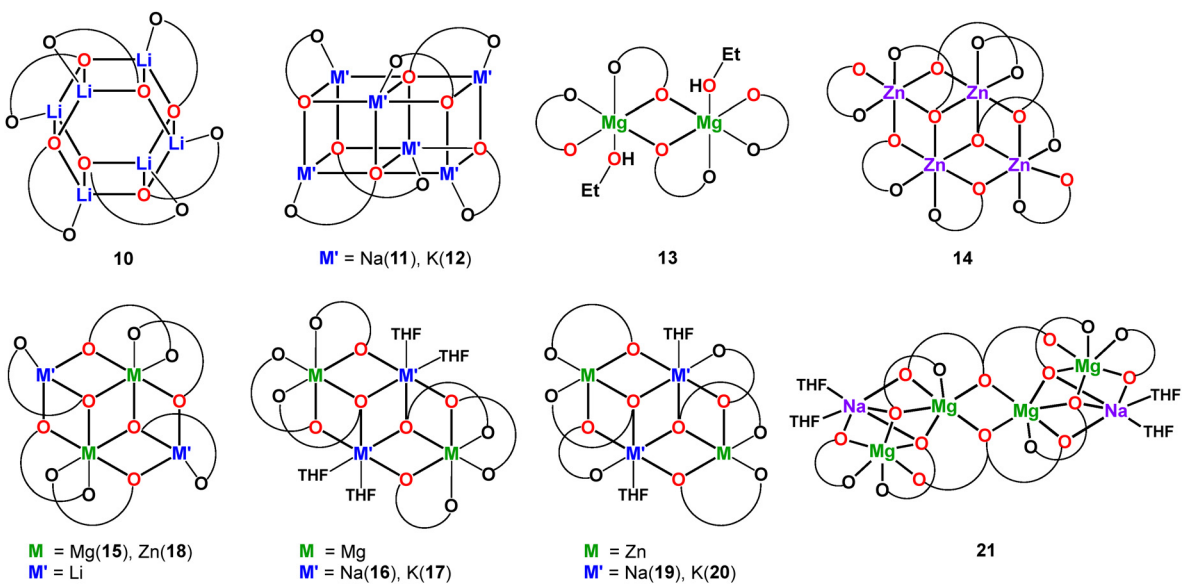

Scheme 5 Homometallic and heterometallic aryloxides **10–21** investigated as catalysts in PA6 alcoholysis.

4-fold increase in **II**, a 2- to 6-fold increase in **III**, no change or up to a 3.5-fold increase in **IV**, a 1.5- to 11-fold increase in **VI**, and a 4- to 8-fold increase in **VII** (ESI, Table S6†). For the catalysts that exhibited the highest activity at 220 °C for 8 h, an extended reaction time of 48 h resulted in a 2- to 8-fold decrease in **V**, likely due to etherification reactions leading to an increased formation of **VI**. These findings suggest that the primary challenge in this process is the generation of a complex mixture of inseparable products (**I–VII**). While increasing the reaction time enhanced polymer degradation, it did not significantly alter the relative composition of individual compounds in the reaction mixture.

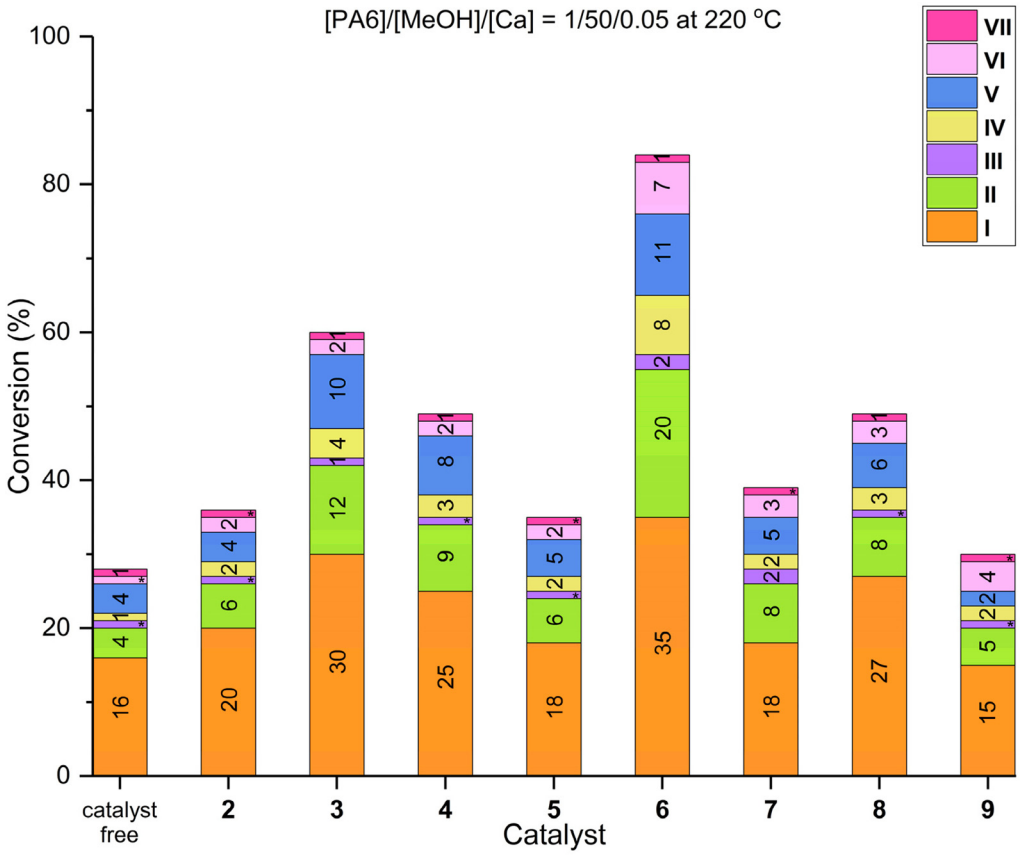

Fig. 17 Catalytic activities of **2–9** in PA6 alcoholysis with stoichiometry [PA6]/[MeOH]/[Ca] = 1/50/0.05 at 220 °C for 8 h. * – Indicates that the content of **III** and **VII** is less than 1%.

When PA6 alcoholysis was performed using benzyl alcohol (BnOH) as the reagent and **13** as the catalyst under the reaction stoichiometry [PA6]/[BnOH]/[M′] = 1/10/0.05 at 220 °C for 25 h, ESI-MS spectra revealed the formation of oligomers X–[HN$(CH_2)_5CO]_n$–O(Bn/H), capped by 6-(dibenzylamino)hexanoyl (**A** and **B** series) and 6-(benzylamino)hexanoyl (**C** series). Additional series (**D**, **E**), generated due to the use of catalyst **13**, supported by EtsalO and EtOH ligands, were also detected in the MS spectra (ESI, Fig. S53†). ^{1}H NMR and FTIR-ATR analysis of the liquid organic products confirmed the presence of low-molecular-weight oligomers (**I**), caprolactam (**II**), *N*-benzylcaprolactam (**III**), benzyl 6-(*N*,*N*-dibenzylamino)caproate (**IV**), and benzyl 6-(*N*-benzylamino)caproate (**IV′**), as shown in Fig. 19 (ESI, Fig. S54–S56†).

The use of excess BnOH also led to the formation of benzyl benzoate and dibenzyl ether. Performing the reaction at 260 °C for 6, 29, or 54 h using **12**, revealed that longer reaction times facilitated the conversion of **I** and **II** into **III** and **IV**. For example, after 6 h, the reaction mixture consisted of **I** (34%), **II** (23%), **III** (17%), **IV** (19%), and **IV′** (7%). After 54 h, the corresponding values were **I** (2%), **II** (9%), **III** (26%), **IV** (56%), and **IV′** (7%) (ESI, Table S7†). Within the group of catalysts investigated for the alcoholysis of PA6 using BnOH, the most efficient were **6** < **10** < **13**, leading to **IV** with a 32–42% content in the reaction mixture. Notably, the heterometallic catalysts **3–5** and **15–20** facilitated the formation of products with a high amount of **I** (51–66%) and a low content of **II** (2–11%) (ESI, Table S8†).

A plausible explanation for the role of metal aryloxides **2–21** in the alcoholysis of PA6 is their ability to increase the porosity of the polymer matrix, thereby enhancing mass transfer and accelerating reaction rates. The observed differences in reactivity among aryloxides **2–21** can be attributed to their varying degrees of migration into the solid PA6, which correlates with the acid–base properties, solubility, and the presence of alkali metal ions in the homometallic and heterometallic aryloxides. Alkali metal aryloxides exhibit greater mobility and are more likely to diffuse into the amorphous regions of PA6. Their higher solubility in MeOH also improves their dispersion, facilitating migration through the polymer and enabling interaction with internal sites. This migration induces local chain mobility or swelling within the polymer, increasing free volume and porosity. Due to their strong basicity and nucleophilicity, alkali metal aryloxides tend to be more ionic and reactive, which promotes chain scission, and depolymerization processes. In contrast, aryloxides of Ca^{2+}, Mg^{2+}, and Zn^{2+} (*e.g.*, **2**, **13**, and **14**) form larger, more tightly bound, and less soluble aggregates, limiting their mobility and penetration

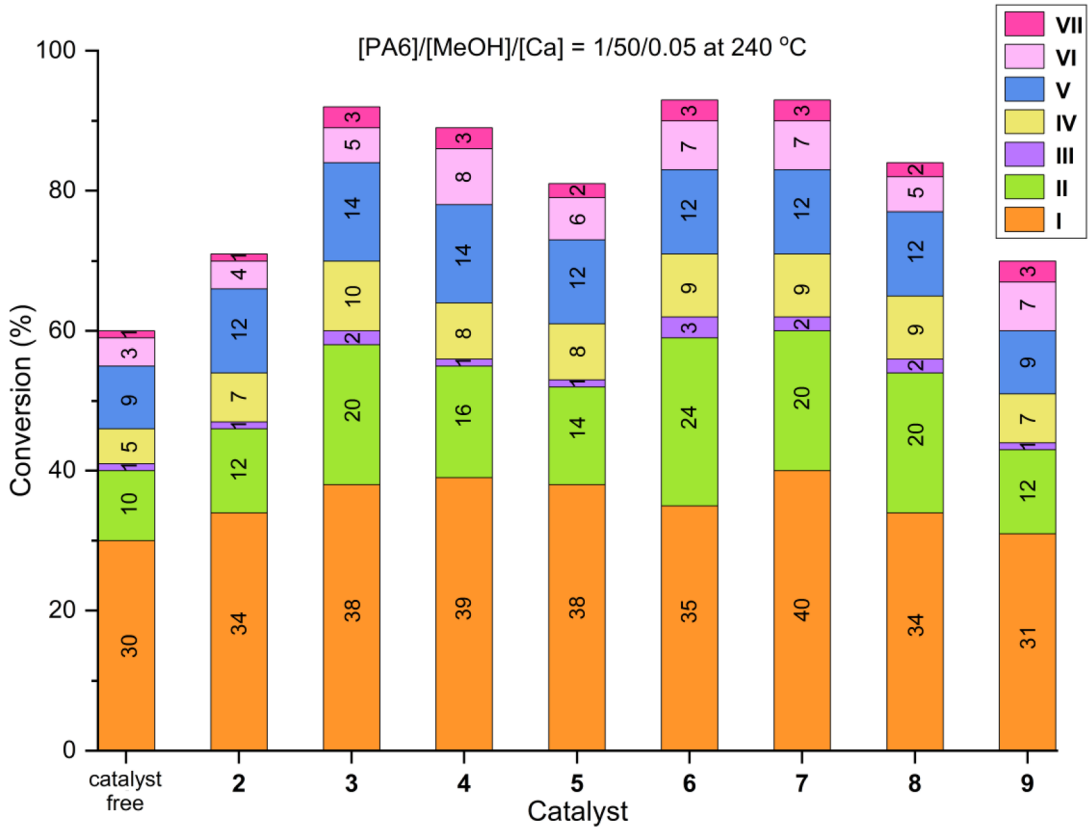

Fig. 18 Catalytic activities of **2–9** in PA6 alcoholysis with stoichiometry [PA6]/[MeOH]/[Ca] = 1/50/0.05 at 240 °C for 8 h.

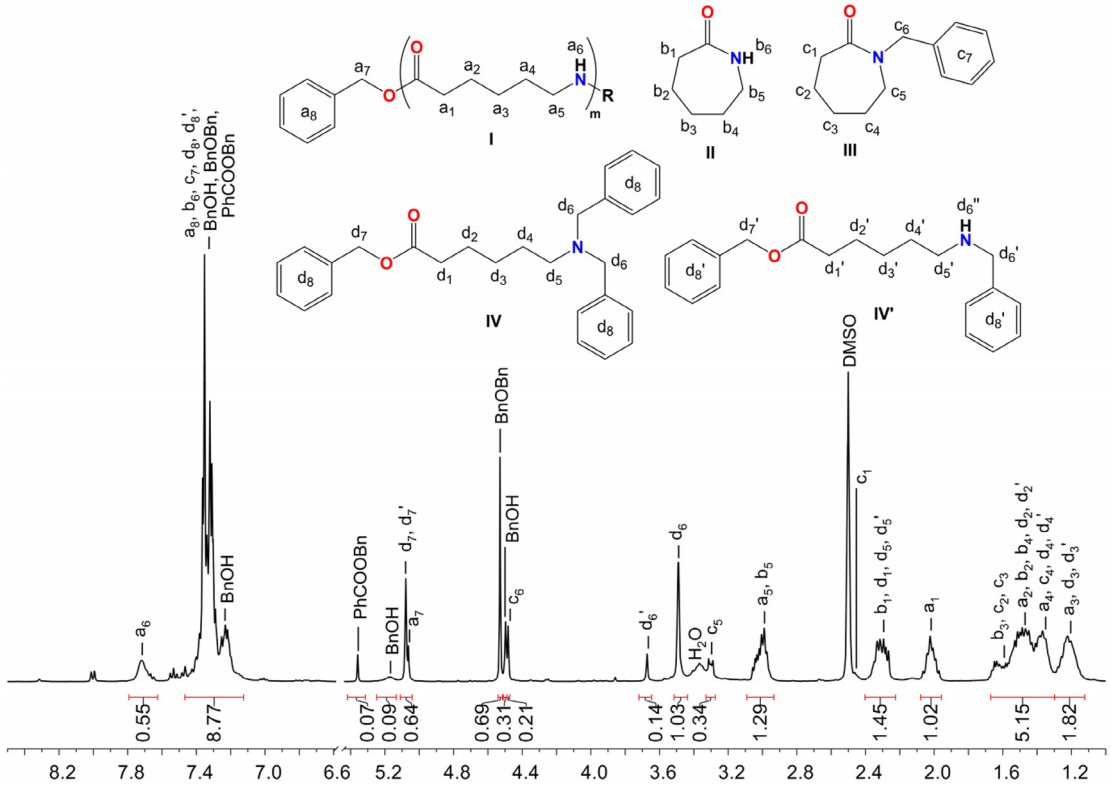

Fig. 19 ^{1}H NMR spectrum of liquid organic products obtained from PA6 alcoholysis using BnOH and **13** as a catalyst after 25 h at 220 °C.

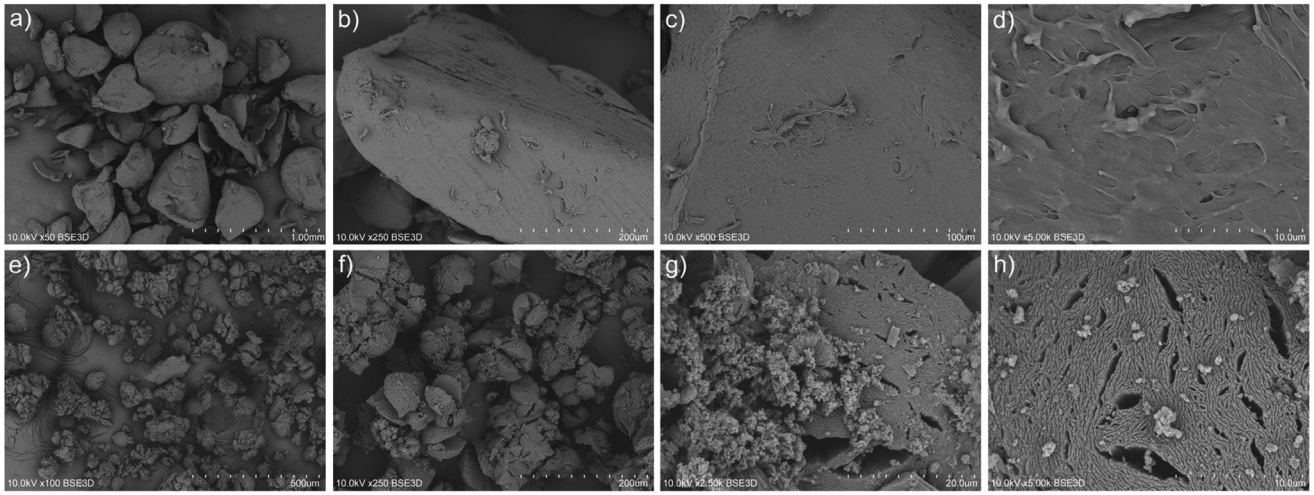

Fig. 20 Comparison of SEM micrographs of virgin PA6 (a–d) with solid residues isolated from reaction mixture (e–h).

into the polymer chains. Heterometallic aryloxide complexes **3–6** and **17–20** generally exhibit even greater solubility in MeOH than their homometallic counterparts, improving their mobility. The presence of divalent metal ions in these heterometallic complexes stabilizes their structural integrity. Furthermore, alkali metal ions in complexes **4–5** and **19–20** are coordinated with THF or MeOH ligands, which can be readily displaced during catalytic process, providing easier access to the polymer backbone. Direct esterification of amides is challenging due to the resonance stabilization of the amide bond and the inherently low nucleophilicity of alcohols. As a result, such reactions typically require harsh conditions and prolonged reaction times.[97] Various strategies have been developed to overcome these challenges, including the use of activating agents,[98] twisted amides,[99] and directing groups. Numerous catalytic systems such as $Sc(OTf)_3$,[100,101] $Ni(cod)_2$/NHC,[102] $FeCl_3{\cdot}6H_2O$,[103] and CeO_2.[104] have also been explored to enhance amide reactivity.

In the present study of PA6 alcoholysis, we propose a mechanism involving amide bond activation *via* coordination of the carbonyl oxygen to Lewis-acidic metal centers. This interaction increases the electrophilicity of the carbonyl carbon, making it more susceptible to nucleophilic attack by MeOH. The resulting addition forms an unstable tetrahedral intermediate that subsequently collapses, leading to cleavage of the amide bond and release of oligomers capped with amine and methyl ester end groups. Such nucleophilic acyl substitution mechanisms have been previously reported for metal complexes with amide ligands, undergoing random esterification upon dissolution in MeOH.[105–109] Mashima and co-workers reported the esterification of *N*,*N*-dialkyl arylamides catalyzed by $[Mn(\mu\text{-}O^nBu)(acac)(Me_2N\text{-}Phen)]_2$ (Me_2N-Phen = 4,7-bis(dimethylamino)-1,10-phe-nanthroline), in which one Mn^{2+} center acted as a Lewis acid by coordinating the amide carbonyl, while the second Mn^{2+} center activated the alcohol nucleophile.[110] More recently, the same group demonstrated that the heterometallic complex $[KMn(\mu\text{-}O^nBu)(\mu\text{-}O^pTol)(acac)(Me_2N\text{–}Phen)]$ exhibits superior catalytic activity, attributed to dual substrate/nucleophile activation occurring exclusively at the Mn^{2+} center.[111]

SEM analysis of the morphology of the PA6 resin used in the reactions revealed a rough and fragmented texture, consisting of irregularly shaped particles with blunt edges and a coarse surface due to mechanical fragmentation (Fig. 20a and b). The analyzed material predominantly exhibits fibrillary structures with a limited number of defects (Fig. 20c and d). In contrast, PA6 residues after alcoholysis show significant morphological alterations compared to the virgin material. The irregularly shaped polymer particles break down into smaller pieces (Fig. 20e and f), exhibiting a rougher surface texture, while low molecular weight products crystallize on the polymer surface. The polymer material begins to crack, with numerous voids and creases appearing due to the loss of structural integrity (Fig. 20g and h), supporting our hypothesis that metal aryloxide catalysts increase the porosity of the polymer matrix and enhance mass transfer.

Conclusion

We describe a simple and convenient solvothermal alcoholysis method for the chemical recycling of post-consumer nylon-6 in the presence of methanol or benzyl alcohol under both catalyst-free and catalytic conditions. A series of homometallic and heterometallic aryloxides, including $[Ca(sal\text{-}Me)_2(MeOH)]_n$ (**1**), $[Ca_3(sal\text{-}Me)_6(MeOH)_2]$ (**2**), $[Ca_2Li_2(sal\text{-}Me)_6(THF)_2]$ (**3**), $[Ca_2Na_2(sal\text{-}Me)_6(MeOH)_4]$ (**4**), $[Ca_2K_2(sal\text{-}Me)_6(MeOH)_4]$ (**5**), $[CaLi_6(sal\text{-}Me)_8]$ (**6**), $[Ca_3Na_4(sal\text{-}Et)_{10}(Hsal\text{-}Et)_2]$ (**7**), $[Ca_4Na(\mu_5\text{-}OH)(sal\text{-}Et)_8(MeOH)]$ (**8**), $[Ca_4K(\mu_5\text{-}OH)(sal\text{-}Et)_8(EtOH)]$ (**9**), $[M'_6(sal\text{-}Me)_6]$ (for M'^+ = Li^+ (**10**), Na^+ (**11**), K^+ (**12**)), $[Mg_2(sal\text{-}Et)_4(EtOH)_2]$ (**13**), $[Zn_4(sal\text{-}Me)_8]$ (**14**), $[M_2M'_2(sal\text{-}Me)_6(THF)_x]$ (for M^{2+} = Mg^{2+} and M'^+ = Li^+ (**15**), Na^+ (**16**), K^+ (**17**); for M^{2+} =

Zn^{2+} and M'^{+} = Li^+ (**18**), Na^+ (**19**), K^+ (**20**); and x = 0, 2, 4), and $[Mg_4Na_2(sal\text{-}Me)_6(sal)_2(THF)_4]$ (**21**) were investigated as catalysts for the depolymerization of polyamide waste. Among this group, heterobimetallic calcium–alkali metal aryloxides (**3–9**) are uncommon examples of molecular aggregates in inorganic structural chemistry, with only 13 known representatives to date.

In reactions conducted with MeOH, PA6 degradation yielded low molecular weight oligomers (**I**), caprolactam (**II**), *N*-methylcaprolactam (**III**), methyl 6-(*N*,*N*-dimethylamino) caproate (**IV**), methyl 6-hydroxycaproate (**V**), methyl 6-methoxycaproate (**VI**), and methyl 5-hexenoate (**VII**). Among the tested catalysts, **6** demonstrated remarkable activity at 200–220 °C. Additionally, binary metal catalysts **3** and **18–20** also exhibited very good catalytic activity in the methanolysis of nylon-6 at 220 °C.

The degradation of PA6 using BnOH led to the formation of **I**, **II**, benzyl derivatives of **III** and **IV**, as well as benzyl 6-(*N*-benzylamino)caproate (**IV′**). Among the catalysts tested for PA6 alcoholysis with BnOH, the most efficient were **6**, **10**, and **13**, yielding **IV** with a content of 32–42% in the product mixture. Furthermore, heterometallic double-open dicubanes **3–5** and **15–20** enabled the formation of products containing a high amount of **I** (51–66%) with a low content of **II** (2–11%) when BnOH was used at 260 °C.

An effective method was developed to convert PA6 waste into a mixture of products **I–VII**, which are well-soluble in low-boiling alcohols, making them attractive for further applications as reagents in the synthesis of polymers and resins of industrial importance.

Experimental section

Materials and methods

All syntheses were performed under a dry N_2 atmosphere using Schlenk techniques. Standard purification methods were applied to the reagents: toluene, hexane, and tetrahydrofuran (THF) were distilled over sodium (Na); CH_2Cl_2 was distilled over phosphorus pentoxide (P_2O_5); and methanol (MeOH) and ethanol (EtOH) were distilled over magnesium (Mg). All chemical reagents were purchased from commercial sources: methyl salicylate (Hsal-Me), metallic calcium, lithium, sodium, and potassium (Sigma-Aldrich); CH_3OH and C_2H_5OH (Stanlab); THF and benzyl alcohol (BnOH, Eurochem BDG); hexane (Chempur); THF-d_8 and $CDCl_3$ (Eurisotop); DMSO-d_6 (Deutero and Eurisotop). Polyamide-6 (PA6) was obtained in the form of commercially available zip ties (for alcoholysis using MeOH) or mowing lines (for alcoholysis using BnOH). ^1H and $^{13}C\{^1H\}$ NMR spectra were recorded at room temperature on JEOL JNM-ECZ 400 MHz, Bruker Avance III 500 MHz, or Bruker Avance 600 MHz spectrometers. Chemical shifts were reported in parts per million (ppm) and referenced to residual protons in deuterated solvents. Compounds **1–9** exhibited moderate solubility in THF-d_8, and due to the presence of trace amounts of the free Hsal-Me ligand – a highly soluble liquid with a high boiling point – it was visible in the ^1H and ^{13}C NMR spectra. FTIR-ATR spectra were recorded on a Bruker Vertex 70 vacuum spectrometer. Elemental analyses were performed using a PerkinElmer 2400 CHN elemental analyzer. ESI-MS data were collected using an XEVO-Waters G3 QTOF mass spectrometer. ESI-MS measurements were performed in a MeOH/H_2O mixture with an additional CH_3CN 0.01% NaOOCH solution. Thermogravimetric analysis (TGA) and differential scanning calorimetry (DSC) measurements were conducted using a TGA/DSC 3+ Mettler-Toledo analyzer. Each analysis was performed in the temperature range of 25–800 °C with a heating rate of 5 °C min^{-1} under a nitrogen (N_2, 6.0) atmosphere (50 mL min^{-1}). The melting temperature (T_m) and degradation temperature (T_d) were determined from the midpoint of the slope change in the curve and from the minima of the endothermic peaks, respectively. Scanning electron microscopy (SEM) imaging of pure PA6 and PA6 residues after alcoholysis was performed using a Hitachi S-3400N microscope equipped with a Thermo Noran System SIX energy dispersive spectroscopy (EDS) system. Single-crystal X-ray diffraction (SCXRD) data were collected using Xcalibur Ruby (compounds **1**, **7**, **8**), SuperNova Dual Atlas (compounds **2–4**), or Kuma KM4 (compounds **6**, **9**) diffractometers at 100 K. Experimental details and crystal data are summarized in Table S1.† The structures were solved by direct methods and refined using the full-matrix least-squares method on F^2 with the SHELXTL software package.[112] Non-hydrogen atoms were refined with anisotropic thermal parameters. Hydrogen atoms were positioned geometrically and included in structure factor calculations but were not refined. Molecular graphics for the resulting structures were created using Diamond (version 3.1e).[113] The crystal of compound **4** was twinned, and its final structure refinement was performed using an HKLF 5 format file generated by CrysAlisPro 1.171.41.80a.

Synthesis and spectroscopic characterization of 1–9

Synthesis of $[Ca(sal\text{-}Me)_2(MeOH)]_n$ (1). To a 150 mL Schlenk flask equipped with a stir bar, metallic calcium (0.2 g, 5.0 mmol) and Hsal-Me (1.3 mL, 10.0 mmol) in MeOH (30.0 mL) were added. The mixture was stirred and heated for 12 h, then concentrated under vacuum to an oily residue and left to crystallize in a refrigerator. The resulting colorless crystals were filtered, washed with hexane (3 × 10 mL), and dried under vacuum. Yield 0.97 g (59%). Anal. calcd for $C_{17}H_{18}O_7Ca$: C, 54.54; H, 4.85. Found: C, 54.57; H, 4.86. ^1H NMR (400 MHz, THF-d_8): δ 7.61 (2H, m, ArH), 7.11 (2H, m, ArH), 6.93 (2H, m, ArH), 6.38 (2H, m, ArH), 3.58 (6H, s, CH_3). ^{13}C NMR (101 MHz, THF-d_8): δ 172.54 (2C, C═O), 171.21 (2C, C–O), 135.35 (2C, Ar), 131.31 (2C, Ar), 124.86 (2C, ArH), 114.72 (2C, Ar), 51.95 (2C, CH_3). FTIR-ATR (cm^{-1}): 3048 (vw), 3022 (w), 2988 (w), 2944 (w), 2896 (vw), 2846 (w), 1914 (vw), 1798 (vw), 1743 (vw), 1657 (vs), 1600 (m), 1543 (m), 1499 (vw), 1469 (m), 1436 (s), 1325 (s), 1263 (m), 1219 (s), 1157 (m), 1085 (m), 1038 (m), 964 (m), 949 (m), 905 (w), 865 (m), 853 (m), 819 (m), 797 (m), 749 (s), 706 (s), 658 (m), 579 (s), 554 (m), 532 (m), 445 (m), 423 (m).

Synthesis of $[Ca_3(sal\text{-}Me)_6(MeOH)_2]$ (2). To a 150 mL Schlenk flask equipped with a stir bar, metallic calcium (0.3 g, 7.5 mmol), Hsal-Me (2.0 mL, 15.0 mmol), THF (20 mL), and MeOH (10.0 mL) were added. The mixture was stirred and heated for 12 h, then concentrated to half of its volume and left to crystallize in a refrigerator. The resulting colorless crystals were filtered, washed with hexane (3 × 10 mL), and dried under vacuum. Yield 1.8 g (66%). Anal. calcd for $C_{50}H_{50}O_{20}Ca_3$: C, 55.04; H, 4.62. Found: C, 55.11; H, 4.64. ^{1}H NMR (400 MHz, THF-d_8): δ 7.73 (3H, d, J = 7.2 Hz, ArH), 7.63 (3H, d, J = 7.2 Hz, ArH), 7.00 (3H, m, ArH), 6.91 (3H, m, ArH), 6.52 (3H, d, J = 8.1 Hz, ArH), 6.40 (3H, m, ArH), 6.33 (3H, d, J = 8.2 Hz, ArH), 6.26 (3H, m, ArH), 3.62 (6H, s, CH_3), 3.40 (12H, s, CH_3), 3.26 (6H, s, MeOH), 2.65 (2H, s, OH). ^{13}C NMR (101 MHz, THF-d_8): δ {172.10, 171.32 (6C, C═O)}, {171.11, 171.00 (6C, C–O)}, 135.05 (6C, ArH), {132.20, 131.95, 131.52 (6C, ArH)}, {124.81, 124.58, 124.28 (6C, ArH)}, {116.56, 115.05 (6C, Ar)}, {114.09, 112.87 (6C, ArH)}, {51.70, 51.46 (6C, CH_3)}, 49.69 (2C, MeOH). FTIR-ATR (cm^{-1}): 3546 (vw), 3329 (vw), 3056 (vw), 3019 (vw), 2995 (vw), 2948 (vw), 2846 (vw), 2674 (vw), 1660 (vs), 1599 (m), 1543 (m), 1468 (s), 1446 (s), 1436 (s), 1325 (s), 1262 (m), 1221 (vs), 1157 (s), 1048 (s), 1037 (m), 965 (w), 864 (s), 818 (m), 797 (w), 754 (vs), 708 (s), 658 (m), 579 (s), 555 (w), 534 (m), 445 (m), 424 (m).

Synthesis of $[Ca_2Li_2(sal\text{-}Me)_6(THF)_2]$ (3). To a 150 mL Schlenk flask equipped with a stir bar, metallic calcium (0.196 g, 4.9 mmol), Hsal-Me (1.9 mL, 14.7 mmol), MeOH (5.0 mL), and THF (25 mL) were added. After 3 h, Li (0.034 g, 4.9 mmol) was introduced. The mixture was stirred and heated for 12 h, then concentrated to half of its volume and left to crystallize in a refrigerator. The resulting colorless crystals were filtered, washed with hexane (3 × 10 mL), and dried under vacuum. Yield 1.6 g (57%). Anal. calcd for $C_{56}H_{58}O_{20}Ca_2Li_2$: C, 58.74; H, 5.11. Found: C, 58.78; H, 5.12. ^{1}H NMR (400 MHz, THF-d_8): δ 7.64 (6H, d, J = 7.2 Hz, ArH), 7.03 (6H, t, J = 7.2 Hz, ArH), 6.70 (6H, m, ArH), 6.21 (6H, t, J = 7.1 Hz, ArH), {3.68, 3.40 (18H, s, CH_3)}. ^{13}C NMR (101 MHz, THF-d_8): δ 173.24 (6C, C═O), 170.80 (6C, C–O), 134.69 (6C, Ar), 131.86 (6C, Ar), 124.70 (6C, Ar), 115.06 (6C, Ar), 111.72 (6C, Ar), 51.12 (6C, CH_3). ^{7}Li NMR (155 MHz, THF-d_8): δ 4.01 (6Li). FTIR-ATR (cm^{-1}): 3024 (w), 2950 (w), 2847 (w), 2658 (vw), 1667 (vs), 1599 (m), 1547 (m), 1469 (m), 1446 (m), 1437 (m), 1320 (m), 1261 (m), 1222 (s), 1193 (m), 1156 (m), 1141 (m), 1083 (m), 1037 (m), 964 (m), 862 (m), 819 (m), 797 (m), 755 (s), 708 (m), 660 (m), 578 (m), 535 (w), 462 (m), 422 (m).

The molecular structure of compound **3** was determined based on studies of **3·2a** cocrystals, which were isolated from the initial reaction stage with a yield of 45%.

Synthesis of $[Ca_2Na_2(sal\text{-}Me)_6(MeOH)_4]$ (4). To a 150 mL Schlenk flask equipped with a stir bar, metallic calcium (0.200 g, 5.0 mmol), Hsal-Me (1.95 mL, 15.0 mmol), THF (30 mL), and MeOH (5.0 mL) were added. After 8 h, metallic sodium (0.115 g, 5.0 mmol) was introduced. The mixture was stirred for 7 h, then concentrated to half of its volume and left to crystallize in a refrigerator. The resulting colorless crystals were filtered, washed with hexane (3 × 10 mL), and dried under vacuum. Yield 1.7 g (59%). Anal. calcd for $C_{52}H_{58}O_{22}Ca_2Na_2$: C, 53.79; H, 5.03. Found: C, 53.82; H, 5.05. ^{1}H NMR (400 MHz, THF-d_8): δ 7.62 (6H, dd, J = 8.0, 1.4 Hz, ArH), 7.02 (6H, t, J = 7.1 Hz, ArH), 6.75 (6H, m, ArH), 6.19 (6H, t, J = 7.2 Hz, ArH), 3.66 (18H, s, CH_3). ^{13}C NMR (101 MHz, THF-d_8): δ 173.33 (6C, C═O), 170.86 (6C, C–O), 134.56 (6C, Ar), 131.87 (6C, Ar), 124.72 (6C, Ar), 115.01 (6C, Ar), 111.69 (6C, Ar), 51.06 (6C, CH_3). FTIR-ATR (cm^{-1}): 3057 (w), 3016 (w), 2983 (w), 2950 (w), 1845 (vw), 1662 (vs), 1598 (m), 1542 (m), 1465 (s), 1447 (s), 1436 (m), 1405 (m), 1317 (m), 1325 (m), 1259 (m), 1219 (s), 1191 (m), 1155 (m), 1138 (m), 1081 (m), 1029 (m), 993 (vw), 965 (vw), 893 (m), 859 (m), 839 (m), 815 (m), 797 (m), 756 (vs), 707 (s), 669 (m), 657 (m), 638 (m), 574 (m), 535 (m), 476 (m), 453 (m), 435 (m), 423 (m).

Synthesis of $[Ca_2K_2(sal\text{-}Me)_6(MeOH)_4]$ (5). To a 150 mL Schlenk flask equipped with a stir bar, metallic calcium (0.204 g, 5.1 mmol) and Hsal-Me (1.97 mL, 15 mmol) in THF (30 mL) and MeOH (5.0 mL) were introduced. After 8 h, metallic potassium (0.199 g, 5.0 mmol) was added. The mixture was stirred for 12 h, concentrated to half of the volume, and left for crystallization in the refrigerator. The colorless polycrystalline powder was filtered off, washed with hexane (3 × 10 mL), and dried under a vacuum. Yield 2.1 g (69%). Anal. calcd for $C_{52}H_{58}O_{22}Ca_2K_2$: C, 52.34; H, 4.90. Found: C, 52.38; H, 4.92. ^{1}H NMR (400 MHz, THF-d_8): δ 7.62 (6H, d, J = 7.1 Hz, ArH), 7.01 (6H, m, ArH), 6.70 (6H, m, ArH), 6.18 (6H, m, ArH), 3.57 (18H, s, CH_3). ^{13}C NMR (101 MHz, THF-d_8): δ 173.34 (6C, C═O), 170.65 (6C, C–O), 134.74 (6C, ArH), 132.05 (6C, Ar), 124.23 (6C, Ar), 115.26 (6C, Ar), 111.48 (6C, Ar), 51.01 (6C, CH_3). FTIR-ATR (cm^{-1}): 3047 (vw), 3019 (w), 2950 (w), 2847 (w), 1664 (vw), 1598 (m), 1543 (m), 1467 (m), 1447 (s). 1436 (s), 1324 (m), 1260 (m), 1219 (s), 1192 (m), 1155 (m), 1141 (m), 1082 (m), 1035 (m), 964 (w), 861 (m), 816 (m), 797 (m), 757 (s), 709 (m), 657 (m), 576 (m), 535 (m), 426 (m).

Synthesis of $[CaLi_6(sal\text{-}Me)_8]$ (6). To a 150 mL Schlenk flask equipped with a stir bar, metallic calcium (0.101 g, 2.5 mmol), Hsal-Me (2.61 mL, 20 mmol), THF (15 mL), and MeOH (5.0 mL) were added. After 0.5 h, Li (0.104 g, 15 mmol) was introduced. The mixture was stirred for 12 h, concentrated to half of the volume, and left for crystallization in the refrigerator. The resulting colorless crystals were filtered, washed with hexane (3 × 10 mL), and dried under vacuum. Yield 2.54 g (78%). Anal. calcd for $C_{64}H_{56}O_{24}CaLi_6$: C, 59.55; H, 4.37. Found: C, 59.57; H, 4.38. ^{1}H NMR (400 MHz, THF-d_8): δ 7.68 (8H, dd, J = 8.1, 1.8 Hz, ArH), 7.07 (8H, ddd, J = 8.7, 6.9, 1.9 Hz, ArH), 6.67 (8H, d, J = 8.5 Hz, ArH), 6.23 (8H, ddd, J = 8.0, 6.9, 1.2 Hz, ArH), 3.72 (24H, s, CH_3). ^{13}C NMR (101 MHz, THF-d_8): δ 173.40 (8C, C═O), 171.03 (8C, C–O), 134.76 (8C, Ar), 131.86 (8C, Ar), 124.48 (8C, Ar), 115.05 (8C, Ar), 111.85 (8C, Ar), 51.14 (8C, CH_3). ^{7}Li NMR (155 MHz, THF-d_8): δ 4.01 (6Li). FTIR-ATR (cm^{-1}): 3062 (vw), 3025 (vw), 2949 (w), 2846 (vw), 1710 (m), 1678 (vs), 1600 (m), 1549 (m), 1471 (m), 1446 (m), 1437 (m), 1317 (s), 1265 (m), 1227 (s), 1195 (m), 1155 (m), 1141 (m), 1082 (m), 1038 (m), 964 (w), 951 (w), 863 (m), 821 (m), 798 (m), 758 (s), 709 (m), 662 (m), 583 (m), 541 (m), 521 (w), 469 (m), 422 (m).

Synthesis of $[Ca_3Na_4(sal\text{-}Et)_{10}(Hsal\text{-}Et)_2]$ (7). To a 150 mL Schlenk flask equipped with a stir bar, metallic calcium (0.1068 g, 2.7 mmol) in MeOH (5.0 mL) was introduced. Once the metallic calcium had fully reacted, metallic sodium (0.0817 g, 3.6 mmol) and Hsal-Me (1.15 mL, 8.9 mmol) in EtOH (15 mL) were added. The mixture was stirred for 12 hours, concentrated to half of its volume, and left to crystallize in the refrigerator. The resulting colorless crystals were filtered off, washed with hexane (3 × 10 mL), and dried under vacuum. Yield: 1.1 g (72%). Due to the high solubility and significant concentration of the free Hsal-Et ligand, which was removed from the Na^+ coordination sphere in solution, spectroscopic analysis was performed on the isostructural compound $[Ca_3Na_4(sal\text{-}Me)_{10}]$. Anal. calcd for $C_{80}H_{70}O_{30}Ca_3Na_4$: C, 55.75; H, 4.09. Found: C, 55.78; H, 4.10. ^{1}H NMR (400 MHz, THF-d_8): δ 7.62 (10H, d, J = 6.5 Hz, ArH), 7.05 (10H, m, ArH), 6.73 (10H, m, ArH), 6.25 (10H, s, ArH), 3.67 (30H, s, CH_3). ^{13}C NMR (101 MHz, THF-d_8): δ 173.47 (10C, C═O), 170.91 (10C, C–O), 134.80 (10C, Ar), 131.66 (10C, Ar), 124.33 (10C, Ar), 114.63 (10C, Ar), 112.21 (10C, Ar), 51.24 (10C, CH_3). FTIR-ATR (cm^{-1}): 3018 (w), 2950 (w), 2845 (w), 2656 (vw), 1664 (vs), 1615 (vw), 1599 (m), 1541 (m), 1466 (m), 1436 (s), 1323 (m), 159 (m), 1217 (s), 1192 (m), 1155 (m), 1141 (m), 1080 (m), 1035 (m), 964 (m), 859 (m), 813 (m), 797 (m), 754 (s), 708 (m), 657 (m), 575 (m), 534 (m), 426 (m).

Synthesis of $[Ca_4Na(\mu_5\text{-}OH)(sal\text{-}Et)_8(MeOH)]$ (8). To a 150 mL Schlenk flask equipped with a stir bar, metallic calcium (0.2622 g, 6.5 mmol) in MeOH (2.0 mL) was added. Once the metallic calcium had fully reacted, metallic sodium (0.0639 g, 1.65 mmol), Hsal-Me (1.7 mL, 13.1 mmol), and H_2O (0.028 mL, 1.6 mmol) in EtOH (25 mL) were introduced. The mixture was stirred for 12 h, concentrated to half of the volume, and left for crystallization in the refrigerator. The colorless crystals were filtered off, washed with hexane (3 × 10 mL), and dried under a vacuum. Yield 1.57 g (62%). Anal. calcd for $C_{73}H_{77}O_{26}Ca_4Na$: C, 56.43; H, 5.00. Found: C, 56.47; H, 5.02. ^{1}H NMR (600 MHz, THF-d_8): δ 7.71 (4H, d, J = 7.6 Hz, ArH), 7.60 (4H, d, J = 7.4 Hz, ArH), 6.95 (4H, t, J = 7.0 Hz, ArH), 6.85 (4H, t, J = 6.9 Hz, ArH), 6.47 (4H, d, J = 8.3 Hz, ArH), 6.34 (4H, t, J = 7.2 Hz, ArH), 6.27 (4H, d, J = 8.3 Hz, ArH), 6.20 (4H, t, J = 7.2 Hz, ArH), 4.06 (1H, s, MeOH), 3.93–3.68 (16H, m, CH_2), 3.35 (3H, d, J = 16.0 Hz, MeOH), 1.06 (24H, m, CH_3). ^{13}C NMR (151 MHz, THF-d_8): δ {172.06, 171.07 (8C, C═O)}, {170.96, 170.55 (8C, C–O)}, {135.01, 134.93 (8C, Ar)}, {132.26, 131.54 (8C, Ar)},{124.48, 124.18 (8C, Ar)}, {116.75, 115.26 (8C, Ar)}, {113.96, 112.75 (8C, Ar)}, {60.97, 60.55 (8C, CH_2)}, 51.40 (2C, MeOH), {14.34, 14.21 (8C, CH_3)}. FTIR-ATR (cm^{-1}): 3571 (w), 3320 (vw), 3053 (w), 3017 (w), 2981 (w), 2932 (vw), 2906 (w), 2781 (vw), 2660 (vw), 1656 (vs), 1599 (m), 1542 (m), 1467 (s), 1446 (m), 1393 (m), 1370 (m), 1335 (m), 1318 (m), 1257 (m), 1216 (s), 1154 (m), 1081 (m), 1038 (m), 1017 (m), 948 (w), 892 (m), 862 (m), 825 (m), 795 (w), 758 (s), 708(m), 658 (m), 580 (m), 554 (w), 536 (m), 466 (m).

Synthesis of $[Ca_4K(\mu_5\text{-}OH)(sal\text{-}Et)_8(EtOH)]$ (9). To a 150 mL Schlenk flask equipped with a stir bar, metallic calcium (0.2427 g, 6.1 mmol) in MeOH (2.0 mL) was introduced. Once the metallic calcium had fully reacted, metallic potassium (0.0595 g, 1.5 mmol), Hsal-Me (1.57 mL, 12.1 mmol) and H_2O (0.026 mL, 1.5 mmol) in EtOH (25 mL) were introduced. The mixture was stirred for 6 h, concentrated to half of the volume, and left for crystallization in the refrigerator. The colorless crystals were filtered off, washed with hexane (3 × 10 mL), and dried under a vacuum. Yield 1.77 g (74%). Anal. calcd for $C_{74}H_{79}O_{26}Ca_4K$: C, 56.12; H, 5.03. Found: C, 56.07; H, 4.99. ^{1}H NMR (400 MHz, CD_3OD): $[Ca_4K(\mu_5\text{-}OH)(sal\text{-}Me)_8(HOEt)]$: δ 7.64 (8H, d, J = 6.8 Hz, ArH), 7.12 (8H, t, J = 7.4 Hz, ArH), 6.71 (8H, J = 8.3 Hz, ArH), 6.34 (8H, t, J = 7.4 Hz, ArH), 3.34 (24H, s, CH_3, sal-Me); $[Ca_4K(\mu_5\text{-}OH)(sal\text{-}Et)_8(HOEt)]$: δ 7.79 (8H, d, J = 6.9 Hz, ArH), 7.13 (8H, m, ArH), 6.76 (8H, d, J = 8.2 Hz, ArH), 6.56 (8H, t, J = 6.7 Hz, ArH), 3.60 (2H, q, J = 7.0, CH_2), 1.17 (3H, t, J = 7.0, CH_3); EtOH(traces): 3.63 (m, CH_2), 1.22 (m, CH_3). ^{13}C NMR (101 MHz, CD_3OD): δ 172.38 (8C, C═O), 172.17 (8C, C–O), 135.64 (8C, Ar), 133.61 (8C, Ar), 132.29 (8C, Ar), 124.38 (8C, Ar), 116.20 (8C, Ar), 113.69 (8C, Ar), 61.40 (8C, CH_2, sal-Et), 49.00 (8C, CH_3, sal-Me), 14.60 (8C, CH_3, sal-Et); EtOH(traces): 58.32 (CH_2), 18.36 (CH_3). FTIR-ATR (cm^{-1}): 3573 (vw), 3552 (vw), 3060 (vw), 3017 (vw), 2987 (vw), 2954 (w), 2847 (vw), 1659 (vs), 1596 (m), 1562 (m), 1541 (m), 1517 (m), 1468 (m), 1446 (m), 1437 (m), 1401 (m), 1372 (w), 1324 (m), 1261 (m), 1219 (s), 1157 (m), 1084 (m), 1039 (m), 965 (w), 948 (w), 882 (m), 864 (m), 818 (m), 796 (w), 754 (s), 708 (s), 658 (m), 580 (s), 554 (w), 534 (m), 448 (m), 422 (m).

Synthesis of $[M'_6(sal\text{-}Me)_6]$ (for $M'^+ = Li^+$ (10), Na^+ (11), K^+ (12)), $[Mg_2(sal\text{-}Et)_4(EtOH)_2]$ (13), $[Zn_4(sal\text{-}Me)_8]$ (14), $[M_2M'_2(sal\text{-}Me)_6(THF)_x]$ (for $M^{2+} = Mg^{2+}$ and $M'^+ = Li^+$ (15), Na^+ (16), K^+ (17); for $M^{2+} = Zn^{2+}$ and $M'^+ = Li^+$ (18), Na^+ (19), K^+ (20); and x = 0, 2, 4), and $[Mg_4Na_2(sal\text{-}Me)_6(sal)_2(THF)_4]$ (21). Compounds **10–21** for catalytic application were synthesized using previously published procedures.[85,86,93,114]

Polyamide-6 alcoholysis procedure

The PA6 processing procedure using MeOH was carried out as follows: In a standard experiment, PA6 (0.5 g, 4.46 mmol, zip ties) was added to 9.2 mL of MeOH and placed in a 25 mL PTFE-lined hydrothermal reactor. The reactions were conducted at 200–240 °C for 8–48 hours using catalysts **2–21** with a molar ratio of [PA6]/[MeOH]/[M/M′] = 1/50/0.05. After the reaction, the mixture was filtered, and excess MeOH was removed by distillation. The remaining PA6 residue was dried and weighed to calculate the conversion yield. The conversion of PA6 into low molecular weight oligomers (**I**), caprolactam (**II**), *N*-methylcaprolactam (**III**), methyl 6-(*N*,*N*-dimethylamino) caproate (**IV**), methyl 6-hydroxycaproate (**V**), methyl 6-methoxycaproate (**VI**), and methyl 5-hexenoate (**VII**) was determined by ^{1}H NMR measurements in DMSO-d_6.

For polymer alcoholysis using benzyl alcohol (BnOH), typically, 0.5 g of PA6 (5 mm-long fragments cut from a nylon-6 fishing line) was placed in a PTFE reaction vessel, and 4.6 mL of BnOH (10 equivalents per polymer unit) along with catalysts **2–21** (5 mol% relative to M^{2+} or M^+ ion) was added. The PA6 alcoholysis was performed at 220–260 °C for 6–54 h, achieving complete conversion of PA6 into a mixture of low molecular

weight oligomers (**I**), caprolactam (**II**), *N*-benzylcaprolactam (**III**), benzyl 6-(*N*,*N*-dibenzylamino)caproate (**IV**), and benzyl 6-(*N*-benzylamino)caproate (**IV′**).

Author contributions

Rafał Petrus: conceptualization, synthesis, investigation (crystal structure solution and refinement of **1–4**), project administration, funding acquisition, writing – original draft, writing – review, and editing. Karolina Matuszak: catalytic applications of **2–21** in the chemical depolymerization of nylon-6 in MeOH, NMR, IR, and MS investigation of organic products, preparation of the ESI file.† Adrian Kowaliński: catalytic applications of **2–21** in the chemical depolymerization of nylon-6 in BnOH, NMR, IR, and MS investigation of organic products, preparation of the ESI file.† Tadeusz Lis: single-crystal X-ray diffraction measurement, solution, and refinement of **6–9**.

Conflicts of interest

The authors declare no conflict of interest.

Data availability

The authors confirm that the data supporting the findings of this study are available within the article and its ESI.† Crystallographic data for the structural analyses reported in this paper have been deposited with the Cambridge Crystallographic Data Centre (CCDC) under accession numbers CCDC 2420420–2420427.†

Acknowledgements

The authors thank the Polish National Science Center for financial support, grant number 2023/49/B/ST4/04068 (RP, AK). This work was also co-financed by an Internal grant Faculty of Chemistry, Wroclaw University of Science and Technology (WUST), titled "*Investigation of Cooperative Effects in Heterometallic Catalysts for the Chemical Recycling of Plastic Waste*" (RP, KM). The authors also acknowledge Dr J. Utko for the synthesis of compounds **8–9**, carried out under contract no. 07/03/K13W03D10/2020 (March 16, 2020 – March 31, 2021), funded by grant number 2017/26/D/ST5/01123.

References

1 T. Li, K. N. McCabe, L. Maron, X. Leng and Y. Chen, Organocalcium Complex-Catalyzed Selective Redistribution of $ArSiH_3$ or $Ar(alkyl)SiH_2$ to Ar3SiH or $Ar_2(alkyl)SiH$, *ACS Catal.*, 2021, **11**, 6348–6356.
2 T. Suzuki, N. Yamagiwa, Y. Matsuo, S. Sakamoto, K. Yamaguchi, M. Shibasaki and R. Noyori, Catalytic asymmetric aldol reaction of ketones and aldehydes using chiral calcium alkoxides, *Tetrahedron Lett.*, 2001, **42**, 4669–4671.
3 S. Sengupta, S. Krieck and M. Westerhausen, In situ Generation of Organocalcium Compounds for a Calcium-Based Grignard-Type Chemistry, *Dalton Trans.*, 2024, **53**, 14961–14965.
4 J. Begouin and M. Niggemann, Calcium–Based Lewis Acid Catalysts, *Chem. – Eur. J.*, 2013, **19**, 8030–8041.
5 S. Harder, From limestone to catalysis: application of calcium compounds as homogeneous catalysts, *Chem. Rev.*, 2010, **110**, 3852–3876.
6 F. Ossola, P. Tomasin, C. De Zorzi, N. E. Habra, M. Chiurato and M. Favaro, New calcium alkoxides for consolidation of carbonate rocks. Influence of precursors' characteristics on morphology, crystalline phase and consolidation effects, *New J. Chem.*, 2012, **36**, 2618–2624.
7 P. Tomasin, G. Mondin, M. Zuena, N. E. Habra, L. Nodari and L. M. Moretto, Calcium alkoxides for stone consolidation: Investigating the carbonation process, *Powder Technol.*, 2018, **344**, 260–269.
8 M. Favaro, M. Chiurato, P. Tomasin, F. Ossola, N. E. Habra, N. Brianese, I. Svensson, E. Beckers, V. J. F. Pérez, M. D. R. Sánchez and A. Bernardi, *Research for development*, Springer, 2014, 413–422.
9 C. Bossard, H. Granel, E. Jallot, V. Montouillout, F. Fayon, J. Soulie, C. Drouet, Y. Wittrant and J. Lao, Mechanism of Calcium Incorporation Inside Sol–Gel Silicate Bioactive Glass and the Advantage of Using $Ca(OH)_2$ over Other Calcium Sources, *ACS Biomater. Sci. Eng.*, 2019, **5**, 5906–5915.
10 D. Caurant and O. Majérus, in *Encyclopedia of Materials: Technical Ceramics and Glasses: Volume 42*, Elsevier, 2021, vol. 2, pp. 762–789.
11 H. D. Kluge and D. Kenneth, *US Pat*, 2870134, 1959, Texaco Inc. (CAN 53:47969).
12 D. Love, *US Pat*, 3657124, 1972, Texaco Inc. (CAN 77:22559).
13 H. Chafetz, W. H. Canning and B. G. Morissette, *US Pat*, 3691076, 1972, Texaco Inc. (CAN 78:46024).
14 Y. Ling, T. Ling, K. Jin and W. Xia, *CN Pat*, 108912355, 2018, Suzhou Youjun Environmental Technology Co., Ltd. (CAN 171:191616).
15 Y. Ling, T. Ling, K. Jin and W. Xia, *CN Pat*, 108676259, 2018, Suzhou Youjun Environmental Technology Co., Ltd. (CAN: 170:605939).
16 H. Ludwig, *DE Pat*, 1071569, 1956, Th. Goldschmidt A.-G. (CAN: 56:32704).
17 F. R. Greenbaum, Calcium salts of low-temperature TAR phenols, *Am. J. Pharm.*, 1927, **99**, 10–12.
18 F. R. Greenbaum, Calcium salts of low-temperature TAR phenols, *Chem. Zentralbl.*, 1925, **96**, 2192.
19 X. Geng, W. Huang, X. Li, R. Liu and H. Xu, Research on the Chemical Precipitation Treatment of Phenolic

Wastewater of Ceramics Factory, *Shandong Chem. Ind.*, 2011, **40**, 13–15.

20 N. Nezafati, S. Hesaraki and M. Shahrezaee, Preparation and Physicochemical Evaluation of Paste-Paste Calcium Hydroxide Based Dental Cement and the Effect of Replacement of Glycol Disalicylate by Methyl Salicylate on its Basic Properties, *Adv. Compos. Lett.*, 2012, **21**, 78–83.

21 T. J. Boyle, B. A. Hernandez-Sanchez, C. M. Baros, L. N. Brewer and M. A. Rodriguez, Influencing the morphology and phase of calcium ceramic nanoparticles based on the calcium alkoxide precursors' characteristics, *Chem. Mater.*, 2007, **19**, 2016–2026.

22 J. Bhattacharjee, A. Sarkar and T. K. Panda, Alkali and Alkaline Earth Metal Complexes as Versatile Catalysts for Ring-Opening Polymerization of Cyclic Esters, *Chem. Rec.*, 2021, **21**, 1898–1911.

23 J. Bhattacharjee, A. Harinath, H. P. Nayek, A. Sarkar and T. K. Panda, Highly Active and Iso-Selective Catalysts for the Ring-Opening Polymerization of Cyclic Esters using Group 2 Metal Initiators, *Chem. – Eur. J.*, 2017, **23**, 9319–9933.

24 K. Devaine-Pressing, F. J. Oldenburg, J. P. Menzel, M. Springer, L. N. Dawe and C. M. Kozak, Lithium, sodium, potassium and calcium amine-bis(phenolate) complexes in the ring-opening polymerization of rac-lactide, *Dalton Trans.*, 2020, **49**, 1531–1544.

25 Y. Sarazin, R. H. Howard, D. L. Hughes, S. M. Humphrey and M. Bochmann, Titanium, zinc and alkaline-earth metal complexes supported by bulky O,N,N,O-multidentate ligands: syntheses, characterisation and activity in cyclic ester polymerisation, *Dalton Trans.*, 2005, 340–350.

26 L. Clark, G. B. Deacon, C. M. Forsyth, P. C. Junk, P. Mountford, J. P. Townley and J. Wang, Synthesis and structures of calcium and strontium 2,4-di-tert-butylphenolates and their reactivity towards the amine co-initiated ring-opening polymerisation of rac-lactide, *Dalton Trans.*, 2013, **42**, 9294–9312.

27 B. Liu, T. Roisnel, J. Guégan, J. Carpentier and Y. Sarazin, Heteroleptic silylamido phenolate complexes of calcium and the larger alkaline earth metals: B–Agostic AE···SI–H stabilization and activity in the Ring–Opening polymerization of L–Lactide, *Chem. – Eur. J.*, 2012, **18**, 6289–6301.

28 R. L. Jones, Z. R. Turner, J.-C. Buffet and D. O'Hare, Phenoxy imine NOON complexes of heavy alkaline earth ions for the ring-opening polymerisation of cyclic esters, *Polym. Chem.*, 2024, **15**, 1767–1776.

29 D. J. Darensbourg, W. Choi, O. Karroonnirun and N. Bhuvanesh, Ring-Opening Polymerization of Cyclic Monomers by Complexes Derived from Biocompatible Metals. Production of Poly(lactide), Poly(trimethylene carbonate), and Their Copolymers, *Macromolecules*, 2008, **41**, 3493–3502.

30 M. Westerhausen, S. Schneiderbauer, A. N. Kneifel, Y. Söltl, P. Mayer, H. Nöth, Z. Zhong, P. J. Dijkstra and J. Feijen, Organocalcium Compounds with Catalytic Activity for the Ring–Opening Polymerization of Lactones, *Eur. J. Inorg. Chem.*, 2003, **2003**, 3432–3439.

31 H.-Y. Chen, L. Mialon, K. A. Abboud and S. A. Miller, Comparative Study of Lactide Polymerization with Lithium, Sodium, Magnesium, and Calcium Complexes of BHT, *Organometallics*, 2012, **31**, 5252–5261.

32 Y. Sarazin, B. Liu, T. Roisnel, L. Maron and J.-F. Carpentier, Discrete, Solvent-Free Alkaline-Earth metal cations: Metal···Fluorine interactions and ROP catalytic activity, *J. Am. Chem. Soc.*, 2011, **133**, 9069–9087.

33 R. Stroh and R. Seydel, *US Pat*, 3051762, 1962, Farbenfabriken Bayer A.-G. (CAN: 58:8670).

34 X. Zheng, J. Huang, Y. Yao and X. Xu, Stoichiometric reactions and catalytic dehydrogenations of amine–boranes with calcium aryloxide, *Chem. Commun.*, 2019, **55**, 9152–9155.

35 T. Tsubogo, Y. Yamashita and S. Kobayashi, Chiral Calcium Catalysts with Neutral Coordinative Ligands: Enantioselective 1,4-Addition Reactions of 1,3-Dicarbonyl Compounds to Nitroalkenes, *Angew. Chem., Int. Ed.*, 2009, **48**, 9117–9120.

36 Y. M. A. Yamada and S. Ikegami, Efficient Baylis–Hillman reactions promoted by mild cooperative catalysts and their application to catalytic asymmetric synthesis, *Tetrahedron Lett.*, 2000, **41**, 2165–2169.

37 G. Kumaraswamy, M. N. V. Sastry, N. Jena, K. R. Kumar and M. Vairamani, Enantioenriched (S)-6,6′-diphenylBinol-Ca: a novel and efficient chirally modified metal complex for asymmetric epoxidation of α,β-unsaturated enones, *Tetrahedron: Asymmetry*, 2003, **14**, 3797–3803.

38 G. Kumaraswamy, M. N. V. Sastry and N. Jena, Calcium-BINOL: a novel and efficient catalyst for asymmetric Michael reactions, *Tetrahedron Lett.*, 2001, **42**, 8515–8517.

39 G. Kumaraswamy, N. Jena, M. N. V. Sastry, M. Padmaja and B. Markondaiah, Enantioenriched Calcium–(R)–5,5′,6,6′,7,7′,8,8′–Octahydro–BINOL (H8-BINOL): an efficient catalyst for the creation of a quaternary stereocenter#, *Adv. Synth. Catal.*, 2005, **347**, 867–871.

40 G. B. Deacon, P. C. Junk, G. J. Moxey, M. Guino-O and K. Ruhlandt-Senge, Metal based synthetic routes to heavy alkaline earth aryloxo complexes involving ligands of moderate steric bulk, *Dalton Trans.*, 2009, 4878–4887.

41 J. Utko, S. Przybylak, L. B. Jerzykiewicz, S. Szafert and P. Sobota, A Family of Group 4 Metal Alkoxo Complexes with an M3(μ3-O) Core Relevant to Ziegler–Natta Catalyst Intermediates, *Chem. – Eur. J.*, 2002, **9**, 181–190.

42 G. B. Deacon, C. M. Forsyth and P. C. Junk, 2,6-Diphenylphenolates of calcium, strontium and barium exhibiting π-phenyl encapsulation of the partially naked cations, *J. Organomet. Chem.*, 2000, **607**, 112–119.

43 W. Teng, M. Guino-O, J. Hitzbleck, U. Englich and K. Ruhlandt-Senge, From monomers to solids: controlled hydrolysis to form novel, heteroleptic Hydroxide-Containing complexes, *Inorg. Chem.*, 2006, **45**, 9531–9539.

44 W. J. Evans, W. G. McClelland, M. A. Greci and J. W. Ziller, The utility of aryl oxide ligands as bridging ligands for

europium and calcium-containing compounds, *Eur. J. Solid State Inorg. Chem.*, 1996, **33**, 145–146.

45 G. B. Deacon, P. C. Junk and G. J. Moxey, Synthesis and structural characterisation of the heavier alkaline earth 2,6-di-iso-propylphenolate complexes, *New J. Chem.*, 2010, **34**, 1731–1736.

46 W. Maudez, M. Meuwly and K. M. Fromm, Analogy of the Coordination Chemistry of Alkaline Earth Metal and Lanthanide Ln2+ Ions: The Isostructural Zoo of Mixed Metal Cages [IM(OtBu)4{Li(thf)}4(OH)] (M=Ca, Sr, Ba, Eu), [MM′6(OPh)8(thf)6] (M=Ca, Sr, Ba, Sm, Eu, M′=Li, Na), and their Derivatives with 1,2-Dimethoxyethane, *Chem. – Eur. J.*, 2007, **13**, 8302–8316.

47 W. Maudez, D. Häussinger and K. M. Fromm, Substitution reactions on CaI2: synthesis of mixed metal Lithium–Calcium–Phenolates, and cluster transformation as a function of solvent, *Z. Anorg. Allg. Chem.*, 2006, **632**, 2295–2298.

48 M. F. Zuniga, G. B. Deacon and K. Ruhlandt-Senge, Developments in Heterobimetallic S-Block Systems: Synthesis and structural survey of molecular M/AE (M = Li, Na, K, CS; AE = Ca, SR) aryloxo complexes, *Inorg. Chem.*, 2008, **47**, 4669–4681.

49 W. Gruszka and J. A. Garden, Advances in heterometallic ring-opening (co)polymerisation catalysis, *Nat. Commun.*, 2021, **12**, 3252.

50 M. Y. Kondo, L. S. Montagna, G. F. de Melo Morgado, A. L. G. de Castilho, L. A. P. dos Santos Batista, E. C. Botelho, M. L. Costa, F. R. Passador, M. C. Rezende and M. V. Ribeiro, Recent advances in the use of Polyamide-based materials for the automotive industry, *Polímeros*, 2022, **32**, e2022023.

51 V. Hirschberg and D. Rodrigue, Recycling of polyamides: Processes and conditions, *J. Polym. Sci.*, 2023, **61**, 1937–1958.

52 P. P. X. Yap, Z. Yen, T. Salim, H. C. A. Lim, C. K. Chung and Y. M. Lam, The impact of mechanical recycling on the degradation of polyamide, *Polym. Degrad. Stab.*, 2024, **225**, 110773.

53 A.-J. Minor, R. Goldhahn, L. Rihko-Struckmann and K. Sundmacher, Chemical recycling processes of nylon 6 to Caprolactam: review and Techno-Economic assessment, *J. Chem. Eng.*, 2023, **474**, 145333.

54 A. Kamimura, K. Ikeda, S. Suzuki, K. Kato, Y. Akinari, T. Sugimoto, K. Kashiwagi, K. Kaiso, H. Matsumoto and M. Yoshimoto, Efficient conversion of polyamides to Ω–Hydroxyalkanoic acids: a new method for chemical recycling of waste plastics, *ChemSusChem*, 2014, **7**, 2473–2477.

55 Z. Liu and Y. Ma, Chemical recycling of Step-Growth polymers guided by Le Chatelier's principle, *ACS Eng. Au*, 2024, **4**, 432–449.

56 C. Mihut, D. K. Captain, F. Gadala-Maria and M. D. Amiridis, Review: Recycling of nylon from carpet waste, *Polym. Eng. Sci.*, 2001, **41**, 1457–1470.

57 M. L. Zheng, M. Wang, Y. Li, Y. Xiong and C. Wu, Recycling and degradation of polyamides, *Molecules*, 2024, **29**, 1742.

58 L. Wursthorn, K. Beckett, J. O. Rothbaum, R. M. Cywar, C. Lincoln, Y. Kratish and T. J. Marks, Selective Lanthanide–Organic catalyzed depolymerization of nylon–6 to E–Caprolactam, *Angew. Chem., Int. Ed.*, 2023, **62**, e202212543.

59 J. M. Harrowfield, R. P. Sharma, B. W. Skelton, P. Venugopalam and A. H. White, Structural systematics of 2/4-Nitrophenoxide complexes of Closed-Shell metal ions. v 2-Nitrophenoxides of group 2, *Aust. J. Chem.*, 1998, **51**, 775–784.

60 S. Gao, L.-H. Huo, J.-W. Liu and S. W. Ng, Twinned poly [[diaquacalcium(II)]-μ4-benzene-1,3-dioxyacetato], *Acta Crystallogr., Sect. E:Struct. Rep. Online*, 2005, **61**, m407–m409.

61 G. Smith, E. J. O'Reilly and C. H. L. Kennard, Structures of the divalent metal complexes with benzene-1,2-dioxydiacetic acid, *Polyhedron*, 1987, **6**, 871–879.

62 T. Hidalgo, L. Cooper, M. Gorman, T. Lozano-Fernández, R. Simón-Vázquez, G. Mouchaham, J. Marrot, N. Guillou, C. Serre, P. Fertey, Á. González-Fernández, T. Devic and P. Horcajada, Crystal structure dependent in vitro antioxidant activity of biocompatible calcium gallate MOFs, *J. Mater. Chem. B*, 2017, **5**, 2813–2822.

63 A. Rosado, O. Vallcorba, B. Vázquez-Lasa, L. García-Fernández, R. A. Ramírez-Jiménez, M. R. Aguilar, A. M. López-Periago, C. Domingo and J. A. Ayllón, Facile, fast and green synthesis of a highly porous calcium-syringate bioMOF with intriguing triple bioactivity, *Inorg. Chem. Front.*, 2023, **10**, 2165–2173.

64 R. M. Main, D. B. Cordes, A. V. Desai, A. M. Z. Slawin, P. Wheatley, A. R. Armstrong and R. E. Morris, Solvothermal synthesis of a novel Calcium Metal-Organic framework: high temperature and electrochemical behaviour, *Molecules*, 2021, **26**, 7048.

65 P.-C. Liang, H.-K. Liu, C.-T. Yeh, C.-H. Lin and V. Zima, Supramolecular Assembly of Calcium Metal–Organic Frameworks with Structural Transformations, *Cryst. Growth Des.*, 2011, **11**, 699–708.

66 W.-D. Song, X.-X. Guo and C.-H. Zhang, Poly[aqua(μ3–3,5-dinitrosalicylato)calcium(II)], *Acta Crystallogr., Sect. E: Struct. Rep. Online*, 2007, **63**, m399–m401.

67 Z.-B. Zhu, W. Wan, Z.-P. Deng, Z.-Y. Ge, L.-H. Huo, H. Zhao and S. Gao, Structure modulations in luminescent alkaline earth metal-sulfonate complexes constructed from dihydroxyl-1,5-benzenedisulfonic acid: Influences of metal cations, coordination modes and pH value, *CrystEngComm*, 2012, **14**, 6675–6688.

68 M. Bolte, CSD Communication (Private Communication) 2020, CCDC 2004914.†

69 G. B. Deacon, P. C. Junk, S. G. Leary and A. Urbatsch, Expanding the series of [RE2CA(OQ)8] structures: new heterobimetallic rare Earth/Alkaline Earth 8-Quinolinolate complexes, *Z. Anorg. Allg. Chem.*, 2012, **638**, 2001–2007.

70 G. B. Deacon, P. C. Junk and S. G. Leary, Novel heterobimetallic Neodymium/Calcium 8-Quinolinolate complexes

prepared directly from the metals, *Z. Anorg. Allg. Chem.*, 2004, **630**, 1541–1543.

71 G. B. Deacon, C. M. Forsyth, P. C. Junk, U. H. Kynast, G. Meyer, J. Moore, J. Sierau and A. Urbatsch, Novel rare earth quinolinolate complexes, *J. Alloys Compd.*, 2007, **451**, 436–439.

72 W.-Y. Zhang, Y.-M. Tian, H.-F. Li, P. Chen, Y.-Q. Zhang, P.-F. Yan and W.-B. Sun, Strictly linear trinuclear Dy–Ca/Mg–Dy single-molecule magnets: the impact of long-range f–f ferromagnetic interactions on suppressing quantum tunnelling of magnetization leading to slow magnetic relaxation, *Dalton Trans.*, 2017, **46**, 8259–8268.

73 S. Yang, X. Ye, Y. Fan, B. Deng, S. Yu, X. Huang and S. Luo, *CN Pat*, 117586816, 2024, Guangxi Beihai Yuchai Petronas High-grade Lubricant Co., Ltd.

74 Y. Xie, F. Huang, X. Huang, C. Lu, Y. Mo, J. Liang, Z. Tong, Z. Zhao, M. Yang, H. Li, X. Tang, M. Su, Z. Tian and M. Lan, *CN Pat*, 102618364, 2012, Guangxi University (CAN 157:360525).

75 R. L. Jones, Z. R. Turner, J.-C. Buffet and D. O'Hare, Bis (phenoxy-imine) Alkaline–Earth Complexes with Competing Binding Pockets, *Organometallics*, 2024, **43**, 414–426.

76 I. E. Nifant'ev, M. E. Minyaev, A. V. Shlyakhtin, P. V. Ivchenko and A. V. Churakov, Bulky ortho -di-substituted phenolates of magnesium, calcium and zinc: structural features and comparison of catalytic properties in polymerization of ε-caprolactone and rac -lactide, *Mendeleev Commun.*, 2017, **27**, 341–343.

77 K. F. Tesh, T. P. Hanusa, J. C. Huffman and C. J. Huffman, Structural relationships between mono- and dimeric bis (alkoxides) and bis(aryloxides) of calcium and barium. X-ray crystal structures of M(OC6H2-tert-Bu2–2,6-Me-4)2 (THF)3.(THF) (M = calcium, barium) and [Ca(.mu.-OR) (OR)(THF)]2.2(toluene) [R = C(C6H5)2CH2C6H4Cl-4], *Inorg. Chem.*, 1992, **31**, 5572–5579.

78 P. B. Hitchcock, M. F. Lappert, G. A. Lawless and B. Royo, The synthesis and structure of the alkaline earth metal organic compounds [M(OAr)2(thf)n][M = Ca, n= 3 (1) or 0; M = Ba, n= 4] and [{Ca(NR2)(μNR2)(thf)}2], and the X-ray structure of (1)(Ar = C6H2But2-2,6-Me-4; R = SiMe3; thf -OC4H8), *J. Chem. Soc., Chem. Commun.*, 1990, 1141–1142.

79 I. V. Basalov, A. A. Kissel, E. N. Nikolaevskaya, N. O. Druzhkov, A. V. Cherkasov, J. Long, J. Larionova, G. K. Fukin and A. A. Trifonov, 2-Imino-2,3-dihydrobenzoxazole—a useful platform for designing rare- and alkaline earth complexes with variable di- and trianionic O,N, N, ligands, *Dalton Trans.*, 2021, **51**, 1995–2004.

80 R. Petrus, J. Utko, R. Gniłka, M. G. Fleszar, T. Lis and P. Sobota, Solvothermal alcoholysis method for recycling High-Consistency silicone rubber waste, *Macromolecules*, 2021, **54**, 2449–2465.

81 D. Xiao, E. Wang, H. An, Z. Su, Y. Li, L. Gao, C. Sun and L. Xu, Rationally designed, polymeric, extended Metal–Ciprofloxacin complexes, *Chem. – Eur. J.*, 2005, **11**, 6673–6686.

82 W. Clegg and G. S. Nichol, CSD Communication (Private Communication), CCDC 2079004.†

83 J. Mota, C. Bravo, C. Santos, P. C. Alves, P. Rijo, A. M. Antunes, L. Grenho, M. H. Fernandes, M. M. Alves and V. André, Eco-friendly fabricated multibioactive Ca(II)-antibiotic coordination framework coating on zinc towards improved bone tissue regeneration, *Colloids Surf., B*, 2022, **221**, 113008.

84 Z.-F. Chen, R.-G. Xiong, J.-L. Zuo, Z. Guo, X.-Z. You and H.-K. Fun, X-Ray crystal structures of Mg2 + and Ca2 + dimers of the antibacterial drug norfloxacin, *Dalton*, 2000, 4013–4014.

85 R. Petrus, P. Fałat and P. Sobota, Use of lithium aryloxides as promoters for preparation of α-hydroxy acid esters, *Dalton Trans.*, 2019, **49**, 866–876.

86 R. Petrus, J. Utko, J. Petrus, M. Awashra and T. Lis, Use of group 13 aryloxides for the synthesis of green chemicals and oxide materials, *Dalton Trans.*, 2022, **51**, 4135–4152.

87 M. A. Singh-Wilmot, R. A. Sinclair, I. A. Kahwa and A. J. Lough, Eu3 + substitutional defects and their effect on the luminescence spectral and decay dynamics of salt-type one dimensional rare earth coordination polymers and trinuclear complexes, *J. Lumin.*, 2016, **182**, 98–106.

88 H. Vincent, F. Labrize and L. G. Hubert-Pfalzgraf, Synthesis and molecular structure of Ba5(μ5-OH)[μ3-OCH (CF3)2]4[μ2-OCH(CF3)2]4 [OCH(CF3)2](THF)4(H_2O)·THF: a source of barium fluoride, *Polyhedron*, 1994, **13**, 3323–3327.

89 L. Huang, S. B. Turnipseed, R. C. Haltiwanger, R. M. Barkley and R. E. Sievers, Synthesis and Structures of Volatile Mononuclear and Pentanuclear Chelates of Barium, *Inorg. Chem.*, 1994, **33**, 798–803.

90 P. Miele, J.-D. Foulon and N. Hovnanian, Soluble and volatile barium aryloxide derivatives: Synthesis and molecular structure of Ba5(μ5-OH)(μ3-OAR)4(μ2-OAR)4 (OAr)(THF)5, [Ba(μ1,μ2-dpm)(dpm)(HOAr)2(THF)]2 and [Ba (H2NCH2CH_2OH)(μ1μ2-H2NCH2CH_2OH) (μ2-OH)(μ2-OAr) (HOAr)]∞ (Ar·C6H3But2–3,5; dpm·ButC(O)CHC(O)But), *Polyhedron*, 1993, **12**, 209–219.

91 K. G. Caulton, M. H. Chisholm, S. R. Drake and K. Folting, Synthesis and structural characterization of the first examples of molecular aggregates of barium supported by aryloxide and alkoxide ligands: [HBa5(O)(OPh)9 (thf)8] and [H3Ba6(O)(OBut)11(OCEt2CH_2O)(thf)3](thf = tetrahydrofuran), *J. Chem. Soc., Chem. Commun.*, 1990, 1349–1351.

92 W. Teng, M. Guino-O, J. Hitzbleck, U. Englich and K. Ruhlandt-Senge, From monomers to solids: controlled hydrolysis to form novel, heteroleptic Hydroxide-Containing complexes, *Inorg. Chem.*, 2006, **45**, 9531–9539.

93 R. Petrus, T. Lis and A. Kowaliński, Use of heterometallic alkali metal–magnesium aryloxides in ring-opening polymerization of cyclic esters, *Dalton Trans.*, 2022, **51**, 9144–9158.

94 B. Yang, Q. Niu, S. Liu, C. Wan, F. Zhao and K. Xu, Three metal organic frameworks of 2,4-dihydroxybenzoic acid:

Synthesis, crystal structure and thermal behavior, *J. Mol. Struct.*, 2022, **1261**, 132943.

95 A. Kamimura, K. Kaiso, S. Suzuki, Y. Oishi, Y. Ohara, T. Sugimoto, K. Kashiwagi and M. Yoshimoto, Direct conversion of polyamides to ω-hydroxyalkanoic acid derivatives by using supercritical MeOH, *Green Chem.*, 2011, **13**, 2055–2061.

96 A. Kamimura, Y. Oishi, K. Kaiso, T. Sugimoto and K. Kashiwagi, Supercritical Secondary Alcohols as Useful Media To Convert Polyamide into Monomeric Lactams, *ChemSusChem*, 2007, **1**, 82–84.

97 D. Ye, Z. Liu, H. Chen, J. L. Sessler and C. Lei, Cesium Carbonate Catalyzed Esterification of N-Benzyl-N-Boc-amides under Ambient Conditions, *Org. Lett.*, 2019, **21**, 6888–6892.

98 T. Toyao, M. N. Rashed, Y. Morita, T. Kamachi, S. M. a. H. Siddiki, M. A. Ali, A. S. Touchy, K. Kon, Z. Maeno, K. Yoshizawa and K. Shimizu, Esterification of Tertiary Amides by Alcohols Through C–N Bond Cleavage over CeO_2, *ChemCatChem*, 2018, **11**, 449–456.

99 G. Li, P. Lei and M. Szostak, Transition-Metal-Free Esterification of Amides via Selective N–C Cleavage under Mild Conditions, *Org. Lett.*, 2018, **20**, 5622–5625.

100 B. N. Atkinson and J. M. J. Williams, Scandium triflate catalyzed ester synthesis using primary amides, *Tetrahedron Lett.*, 2014, **55**, 6935–6938.

101 Y. Kita, Y. Nishii, A. Onoue and K. Mashima, Combined catalytic system of scandium triflate and boronic ester for amide bond cleavage, *Adv. Synth. Catal.*, 2013, **355**, 3391–3395.

102 J. E. Dander and N. K. Garg, Breaking Amides using Nickel Catalysis, *ACS Catal.*, 2017, **7**, 1413–1423.

103 X. Chen, S. Hu, R. Chen, J. Wang, M. Wu, H. Guo and S. Sun, Fe-catalyzed esterification of amides via C–N bond activation, *RSC Adv.*, 2018, **8**, 4571–4576.

104 S. M. a. H. Siddiki, A. S. Touchy, M. Tamura and K.-I. Shimizu, Versatile and sustainable alcoholysis of amides by a reusable CeO_2 catalyst, *RSC Adv.*, 2014, **4**, 35803–35807.

105 P. Nanjappan and A. W. Czarnik, Metal ion catalyzed reactions of acrylonitrile, acrylamide, and ethyl acrylate by way of their Diels-Alder cycloadducts, *J. Am. Chem. Soc.*, 1987, **109**, 1826–1833.

106 M. a. R. Raycroft, C. I. Maxwell, R. a. A. Oldham, A. S. Andrea, A. A. Neverov and R. S. Brown, Trifunctional metal Ion-Catalyzed solvolysis: CU(II)-Promoted methanolysis of N,N-bis(2-picolyl) benzamides involves unusual Lewis acid activation of substrate, delivery of coordinated nucleophile, powerful assistance of the leaving group departure, *Inorg. Chem.*, 2012, **51**, 10325–10333.

107 M. C. Bröhmer, S. Mundinger, S. Bräse and W. Bannwarth, Chelating Carboxylic Acid Amides as Robust Relay Protecting Groups of Carboxylic Acids and their Cleavage under Mild Conditions, *Angew. Chem., Int. Ed.*, 2011, **50**, 6175–6177.

108 E. Szajna-Fuller, G. K. Ingle, R. W. Watkins, A. M. Arif and L. M. Berreau, Amide Hydrolysis Reactivity of a N4O-Ligated Zinc Complex: Comparison of Kinetic and Themodynamic Parameters with Those of the Corresponding Amide Methanolysis Reaction, *Inorg. Chem.*, 2007, **46**, 2353–2355.

109 S. Kawaguchi and K. Araki, Mild, rapid and selective alcoholysis of terpyridine-appended amide substrates by Cu2+-catalysis: protonation state and reactivity of the complex, *Inorg. Chim. Acta*, 2005, **358**, 947–956.

110 K. Mashima, Y. Nishii, S. Akiyama and Y. Kita, Manganese (II)-Catalyzed Esterification of N-β-Hydroxyethylamides, *Synlett*, 2015, 1831–1834.

111 T. Hirai, D. Kato, B. K. Mai, S. Katayama, S. Akiyama, H. Nagae, F. Himo and K. Mashima, Esterification of tertiary amides: Remarkable additive effects of potassium alkoxides for generating hetero Manganese–Potassium dinuclear active species, *Chem. – Eur. J.*, 2020, **26**, 10735–10742.

112 G. M. Sheldrick, *Acta Crystallogr., Sect. C: Cryst. Struct. Commun.*, 2015, **71**, 3–8.

113 K. Brandenburg, *DIAMOND, Crystal Impact GbR*, Bonn, Germany, 2007.

114 R. Petrus, K. Matuszak and V. Kinzhybalo, Synthesis of ω-Hydroxy Fatty Acid Alkyl Esters by Macrocyclic Lactones Alcoholysis Catalyzed by Homoleptic and Heteroleptic Zinc Aryloxides, *Chem. – Asian J.*, 2024, **19**, e202400526.

